High-precision U–Pb geochronology of the Lundy igneous complex: implications for North Atlantic volcanism and the far-field Paleocene–Eocene ash record

Karlo Lisica[1,2]*, Lars E. Augland[1], John A. Stevenson[3], Dougal A. Jerram[1,4], Adam Beresford-Browne[5] and Morgan T. Jones[6]

[1] Department of Geosciences, University of Oslo, PO Box 1028 Blindern, 0315 Oslo, Norway
[2] Scottish Universities Environmental Research Centre, Rankine Avenue, Scottish Enterprise Technology Park, East Kilbride G75 0QF, UK
[3] British Geological Survey, The Lyell Centre, Edinburgh EH14 4BA, UK
[4] DougalEARTH Ltd, 31 Whitefields Crescent, Solihull B91 3NU, UK
[5] School of Geography, Earth and Environmental Sciences, University of Birmingham, Edgbaston B15 2TT, UK
[6] Department of Ecology and Environmental Science, University of Umeå, Linnaeus väg 4–6, 907 36 Umeå, Sweden
KL, 0000-0002-6769-3564; LEA, 0000-0001-6033-2734; JAS, 0000-0002-2245-1334; DAJ, 0000-0003-0043-4426; ABB, 0000-0001-9783-8341; MTJ, 0000-0003-3047-0751
* Correspondence: k.lisica.1@research.gla.ac.uk; lisica.karlo@gmail.com

Abstract: The Lundy Island (Bristol Channel, UK) granite is a felsic expression of the southernmost igneous centre of the North Atlantic Igneous Province that emplaced millions of cubic kilometres of magma during the Paleogene. The granite's distinctive S-type, peraluminous, two-mica ± garnet ± tourmaline composition has led to the hypothesis that eruptions from the Lundy volcanic centre may be the source of thick felsic ash layers within the early Eocene Fur Formation (Denmark) that act as key marker horizons for the onset and duration of the Paleocene–Eocene Thermal Maximum. This paper presents high-precision zircon U–Pb emplacement ages of 57.24 ± 0.11/0.12/0.13 Ma for the granite and 55.970 ± 0.021/0.030/0.070 Ma for a felsic 'lundyite' dyke. Trace and rare earth element patterns indicate close similarities between late-stage Lundy activity and ash layer −33 in Denmark. This ash layer was deposited during the Paleocene–Eocene Thermal Maximum carbon isotope excursion, suggesting that the Lundy volcanic centre is likely to be the source of this key ash horizon and that magmatism at Lundy likely continued into the early Eocene.
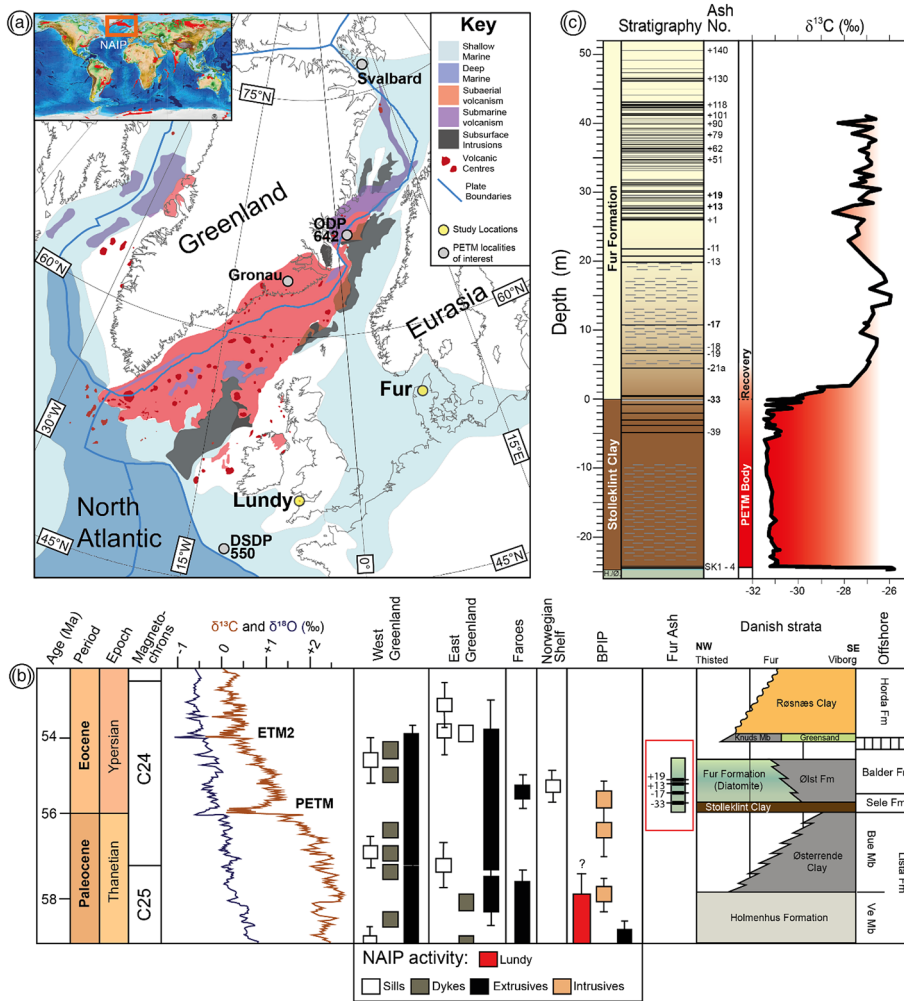
The North Atlantic Igneous Province (NAIP) is one of the largest and best-studied large igneous provinces in the Phanerozoic, with an estimated total magma emplacement volume of 6.6×10^6 km^3 (Bryan and Ernst 2008). It consists of extensive flood basalt provinces and associated intrusions and dykes extending over a vast area that includes east and west Greenland, the Faroe Islands, the Norwegian continental margin, Rockall Bank and the British Isles (Fig. 1; Saunders *et al.* 1997; Storey *et al.* 2007*b*; Bryan and Ernst 2008; Horni *et al.* 2017).

Current geochronological data suggest that the NAIP was emplaced between 64 and 50 Ma (Wilkinson *et al.* 2017), but the main acme of volcanism was confined to between 56 and 54 Ma (e.g. Jerram and Widdowson 2005; Ganerød *et al.* 2010; Larsen *et al.* 2016; Wilkinson *et al.* 2017). This voluminous peak in magmatic activity coincided with active continental break-up between Greenland and Eurasia (Storey *et al.* 2007*b*; Larsen *et al.* 2016) and the hothouse Paleogene climate, including the Paleocene–Eocene Thermal Maximum (PETM). Eruptive activity was dominated by effusive continental flood basalt volcanism (Fig. 1; Storey *et al.* 2007*a*, *b*; Abdelmalak *et al.* 2019; Jolley *et al.* 2021), but the emplacement of the NAIP was also marked by significant explosive volcanism, as evidenced by hundreds of tephra layers deposited in sediments across NW Europe (Morton and Knox 1990; Larsen *et al.* 2003; Egger and Brückl 2006; Storey *et al.* 2007*a*). Ash horizons often contain primary crystals that can be dated using U–Pb and Ar–Ar methods, making them powerful geochronological

marker horizons. Improved radiometric ages for different suites of volcanic and magmatic products will help constrain the absolute and relative timings of key events, such as elevated volcanic activity, global climate change and regional changes (e.g. tectonic uplift).

One locality that shows great promise for tephrostratigraphy during the emplacement of the NAIP is the island of Fur in NW Denmark, where more than 180 ash layers are preserved in a *c.* 75 m sequence of clay and diatomite strata pre- to post-PETM in age (Fig. 1; Jones *et al.* 2019, 2023; Stokke *et al.* 2020*a*, *b*, 2021). These ash layers are named by their number in the stratigraphy, ranging from −39 to +140 (Bøggild 1918). Most of these ash layers are tholeiitic basalts, likely the result of explosive hydromagmatic eruptions (Stokke *et al.* 2020*b*). There are a few felsic tephra layers, including the thick (14 cm) marker horizon named ash layer −33 that was deposited during the PETM carbon isotope excursion at Fur Island (Jones *et al.* 2019), and later ash layers −17, +13 and +19 in the early Eocene stratigraphy.

Obtaining radiometric ages from the ash layers in the Fur strata has proved challenging because northern Denmark was >700 km from the nearest known NAIP source volcano at the time of deposition (Stokke *et al.* 2020*b*). The fine-grained nature of these airfall deposits has hindered successful geochronological efforts. Thus far, only ash layer −17 has been successfully dated to 55.48 ± 0.12 Ma using the Ar–Ar method on sanidine (Storey *et al.* 2007*a*), corrected to the 28.201 Ma Fish Canyon Tuff calibration (Kuiper *et al.* 2008). The deposition age of ash layer −33 is estimated to be *c.*

Fig. 1. (**a**) Plate reconstruction showing the known extent of the North Atlantic Igneous Province at 56 Ma. The palaeoshoreline data are compiled from Abdelmalak *et al.* (2016), Golonka (2009), Hovikoski *et al.* (2021) and Zacke *et al.* (2009). Dark red points denote volcanic centres that are potential sources of volcanic ash. (**b**) Compilation of stable isotope palaeoclimate data (Cramer *et al.* 2009; Littler *et al.* 2014), current radiometric ages of North Atlantic Igneous Province activity (Wilkinson *et al.* 2017; Drake *et al.* 2022) and North Sea stratigraphy (Heilmann-Clausen *et al.* 1985; King 2016) in relation to the GTS2020 geological timescale (Speijer *et al.* 2020). BPIP, British Paleogene Igneous Province; ETM2, Eocene Thermal Maximum 2; NAIP, North Atlantic Igneous Province; PETM, Paleocene–Eocene Thermal Maximum. (**c**) Simplified stratigraphic log of the Stolleklint Clay and the Fur Formation in Denmark in relation to the PETM (Stokke *et al.* 2021; Jones *et al.* 2023). Ashes numbered from −39 to +140, with four (SK1–SK4) found in pre-PETM strata (Jones *et al.* 2019). The felsic ashes investigated in this study (ash layers −33, −17, +13 and +19) are marked in bold. Source: part (a) adapted from Jones *et al.* (2023).

55.8 Ma based on its position within the PETM carbon isotope excursion relative to a U–Pb-dated ash layer in Svalbard (Charles *et al.* 2011; Jones *et al.* 2023). Ash layers +13 and +19 are constrained using cyclostratigraphy to *c.* 180 and *c.* 200 kyr, respectively, after the eruption of ash layer −17 (Westerhold *et al.* 2009). If the source volcanoes of the key tephra layers can be identified, then radiometric dating of these macrocrystalline magmas can give much more precise and robust ages of volcanic and magmatic activity. These refined ages can subsequently be used to constrain how the regional tectonic changes affected NAIP activity in the late Paleocene and early Eocene, and potentially refine the timing and duration of the PETM.

Thus far, the source volcanoes of the key felsic ash layers within the Danish strata are not well constrained. There is convincing geochemical and geochronological evidence that ash layer −17 is the same event as an ignimbrite layer that outcrops close to the top of the continental flood basalts at the Gronau Nunatak in east Greenland (Fig. 1; Heister *et al.* 2001; Larsen *et al.* 2003; Storey *et al.* 2007a). The sources of ash layers −33, +13 and +19 are postulated to be from the British Paleogene Igneous Province (BPIP), an off-axis component of the NAIP (Larsen *et al.* 2003). Numerous volcanic centres are located throughout the BPIP (Fig. 1), with several that evolved magmatic compositions that are now preserved as granite intrusions of various geochemical affinities, as well as ignimbrites and tephra layers (e.g. Emeleus *et al.* 2005). However, the majority of the existing geochronological data from volcanic centres exposed across the British Isles are mid-Paleocene (62.5–58 Ma) in age (Hamilton *et al.* 1998; Chambers *et al.* 2005; Storey *et al.* 2007b; Troll *et al.* 2008; Ganerød *et al.* 2011). There is scattered evidence of latest Paleocene to maybe Eocene silicic

volcanism from centres such as Skye (e.g. Drake *et al.* 2022) and the Mourne Mountains (e.g. Gamble *et al.* 1999), but the current geochronological dataset is sparse.

We investigated the magmatic rocks exposed on Lundy Island, Bristol Channel, UK as a potential source of the felsic ashes exposed in early Eocene strata in Denmark. Lundy Island is dominated by a granitic intrusive complex that is the southernmost outcrop of the BPIP (Figs 1, 2). The Lundy granite has previously been dated using Rb–Sr whole-rock methods, giving an age of 58.7 ± 1.6 Ma (Thorpe *et al.* 1990) when combined with earlier whole-rock and mineral analyses of granites and dolerites (Edmonds *et al.* 1979). The most recent age estimate using U–Pb zircon secondary ion mass spectrometry resulted in ages of 59.8 ± 0.4 to 58.4 ± 0.4 Ma for the granite and 57.3 ± 0.8 and 57.2 ± 0.5 Ma for two felsic dykes (Charles *et al.* 2017). These ages confirm that the Lundy granite complex was active in the late Paleocene, but the data are not sufficiently resolved to evaluate whether there was any temporal overlap of magmatic activity at Lundy with the Paleocene–Eocene boundary.

Larsen *et al.* (2003) showed geochemical similarities between the Lundy granite and felsic dykes with some silicic ash layers at Fur Island (i.e. ash layers −33, +13 and +19). The main Lundy granite body has S-type characteristics and geochemical affinities: it is peraluminous with high Al, high Rb, high Rb/Sr ratios and high trace alkali, Nb and U contents (Thorpe *et al.* 1990; Thorpe and Tindle 1992; Larsen *et al.* 2003; Charles *et al.* 2017). This unique geochemistry differs from the dominantly A-type, metaluminous affinities of the other major granite intrusions within the BPIP (e.g. Stone 1990; Thorpe *et al.* 1990). This led to the Lundy igneous complex being proposed as a potential source for the felsic ashes in

Denmark because ash layer −33 in particular has a distinctive peraluminous geochemical signature, with low Sr, Zr, La, Ce and Y, and high P (Larsen *et al.* 2003), characteristic of S-type granites (Chappell and White 2001; Frost *et al.* 2001).

The Lundy granite is currently one of the only known peraluminous centres active in the late Paleocene and is one of the closest NAIP centres to Denmark, albeit still 1100 km away. This suggests that the complex may be the source of one or several of the ash layers in Danish strata (Larsen *et al.* 2003), but the current geochronological and geochemical datasets are insufficient to corroborate this hypothesis. This study presents new high-precision ages for the Lundy granite and a cross-cutting lundyite dyke, analysing zircons by high-precision U–Pb chemical abrasion isotope dilution thermal ionization mass spectrometry (CA-ID-TIMS). We combine these refined ages with new and existing geochemical data for the Lundy complex and four key felsic ash horizons on Fur Island, Denmark (ash layers −33, −17, +13 and +19). This allows us to assess whether the Lundy magmatic rocks could represent intrusive counterparts to these early Eocene-age eruptions.

Materials and methods

Sample collection and description

Rock samples were collected from ten locations on Lundy Island in September and October 2020 for geochronological and geochemical analyses (Fig. 2, Table 1). The Lundy granite is relatively homogenous, consisting mostly of megacrystic two-mica granite (sample localities OS-LD1, OS-LD2, OS-LD7 and OS-LD9 in this study; Fig. 2), with occurrences of medium- to fine-grained granite (OS-LD8, Fig. 2) and pegmatite-like granites (OS-LD6; Fig. 2) as

layers or pods within the main facies. The Lundy granite shows layering at some locations (OS-LD1, OS-LD2 and OS-LD6; Fig. 2), a result of weathering enhancing the existing laccolith features (Bott *et al.* 1958). Initial mapping described two main types of granite exposure named G1 and G2 (Dollar 1941), but these are chemically homogeneous (Stone 1990; Thorpe *et al.* 1990) and not possible to distinguish by mapping in the field (Charles *et al.* 2017). Cross-cutting microgranite dykes were named G3 (Dollar 1941) and appear to be chemically different from the main granite (Stone 1990; Thorpe *et al.* 1990). However, none of these studies gave localities for the G3 microgranite outcrops and we were unable to locate any given the limited time available for sampling during the COVID-19 pandemic.

The granite is cut by more than 200 dykes, most of which are mafic in composition (OS-LD5; Fig. 2; Dollar 1941) and indicate prolonged activity of the igneous complex. We sampled one felsic dyke found in the south of the island next to the pier (OS-LD10; Fig. 2), colloquially known as 'lundyite' (Hall 1915), which we use to differentiate between other dyke suites. The OS-LD10 sample is a highly weathered, aphanitic, pale greenish grey rock (Fig. 2) with a NE–SW-trending orientation. The lundyite dyke was targeted as a potential source for zircons to help provide the precise age for the late-stage activity on Lundy. The bimodal NE–SW and NW–SE orientation of the dykes (Fig. 2) is interpreted to be the result of NAIP uplift and Alpine-related compression and is found in other intrusive BPIP centres active during the Paleocene–Eocene (Roberts and Smith 1994; Cooper *et al.* 2012; Anderson 2013; Anderson *et al.* 2018). The granite sample OS-LD1 was collected from the same locality as sample LY29 of Charles *et al.* (2017; Fig. 2), whereas the lundyite sample OS-LD10 was collected from the same outcrop as previous samples LY13 of Charles *et al.* (2017) and LUN4 and LUN23 of Thorpe and Tindle (1992).
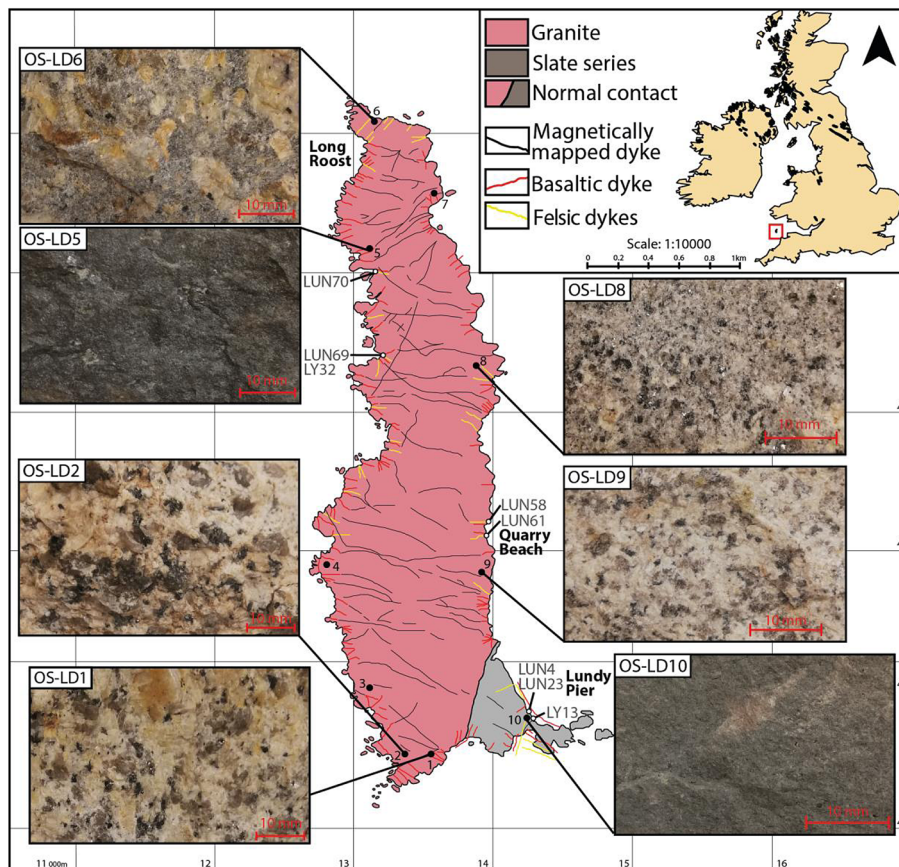
Fig. 2. Geological map of Lundy Island. Most of the island outcrops are granite (pink), although the southern tip is part of the Devonian slate series (grey). Data on magnetically mapped dykes are from Roberts and Smith (1994). Sample localities 1–10 are marked on the map, along with images at those locations to show the representative igneous textures. OS-LD1 and OS-LD2 show the main two-mica ± garnet ± tourmaline granitic texture that comprises *c.* 90% of the exposures. There are sporadic occurrences of medium- to fine-grained granites (represented by OS-LD8 and OS-LD9) and pegmatite-like granites (represented by OS-LD6). OS-LD5 is a cross-cutting dolerite dyke and OS-LD10 is the lundyite dyke exposed near the pier. Also marked on the map are the sample localities of felsic dykes from Thorpe and Tindle (1992) and Charles *et al.* (2017) and the key localities described by Dollar (1941). Samples LUN4 and LUN23 are from the same lundyite dyke as OS-LD10 (this study) and possibly also LY13 (Charles *et al.* 2017). Samples LUN58 and LUN61 are trachyte dykes exposed at Quarry Beach on the east coast. Samples LUN69 and LUN70 exposed on the west coast are described as low-Zr rhyolites (Thorpe and Tindle 1992), with the former from the same dyke as LY32 (Charles *et al.* 2017). Source: geological map adapted from Charles *et al.* (2017).

Zircon extraction and CA-ID-TIMS geochronology

One southern granite sample (OS-LD1) and one lundyite dyke sample (OS-LD10) were used to determine the age of emplacement for the main phase of the Lundy granite complex and later intrusive activity. The samples were crushed and pulverized before the heavy minerals, including zircons, were separated using standard heavy liquid and magnetic methods. Around 100 zircons were chosen from OS-LD1 and OS-LD10 for cathodoluminescence imaging on a scanning electron microscope at the University of Oslo, Norway. Subsequently, 13 zircons from the two samples were selected for CA-ID-TIMS analyses based on texture and morphology. The zircons were annealed for *c.* 72 h at *c.* 900°C (Huyskens *et al.* 2016) and chemically abraded with HF (+HNO_3) at *c.* 195°C for 14 h (Mattinson 2005). The zircon grains in HF were converted to HCl, evaporated and then washed with multiple cycles of HNO_3 before dissolution. The zircons chosen for analyses were spiked with a mixed ^{205}Pb–^{233}U–^{235}U tracer (ET535) (Condon *et al.* 2015). After spiking, the zircons were dissolved in HF and HNO_3 at *c.* 210°C for >48 h in Teflon microcapsules enclosed in a Teflon bomb.

The solutions were chemically separated through chromatography, separating U and Pb from the rare earth elements (REEs) and other ionization-inhibiting elements (Krogh 1973), before being evaporated down and loaded onto zone-refined Re filaments with Si gel. The samples were measured on a Finnigan MAT262 thermal ionization mass spectrometer at the University of Oslo. For all samples, Pb was measured in the dynamic mode on a Masscom secondary electron multiplier and U was measured in the static mode on Faraday cups (apart from some of the smallest inherited zircons, where U was measured in the dynamic mode). Corrections for Pb fractionation were made using the measured long-time average Pb fractionation determined from measurements of the NBS982 Pb standard solution (0.16% per a.m.u. ±0.06%; 2σ). U fractionation was determined from the measured $^{233}U/^{235}U$ ratio. The raw data were reduced using Tripoli (Bowring *et al.* 2011) and the analytical errors and corrections (including tracer uncertainties and Th corrections, assuming a Th/U ratio in the magma of 3 ± 0.5) were incorporated and propagated using an Excel macro based on published algorithms (Schmitz and Schoene 2007). The ages were calculated using Isoplot (Ludwig 2012) with specified decay constants (Jaffey *et al.* 1971). The data are reported in Table 1. The weighted mean errors are reported as ±*x*/*y*/*z*, where *x* represents the analytical uncertainties, *y* represents the *x* + tracer calibration uncertainties and *z* represents the *x* + *y* + uncertainty in the decay constant. The raw data are available in the Supplementary files.

Whole-rock geochemistry

Selected samples of granite (OS-LD2, OS-LD7) and the dolerite (OS-LD5) and lundyite (OS-LD10) dykes were crushed, pulverized and analysed for whole-rock chemistry at ALS Geochemistry, Sweden. The major and trace element and REE abundances were determined using inductively coupled plasma mass spectrometry. Samples of ash layers −33, −17, +13 and +19 were collected from outcrop exposures on Fur Island in Denmark (Fig. 1). These were also pulverized and analysed using the 4Lithores method (lithium metaborate/tetraborate fusion – inductively coupled plasma and inductively coupled plasma mass spectrometry) by Activation Laboratories Ltd for both major and trace elements. Geochemical data from previous studies of Lundy rocks (Stone 1990; Thorpe *et al.* 1990; Thorpe and Tindle 1992) and Danish ash layers (Larsen *et al.* 2003) were incorporated into the dataset. Full geochemical data can be found in the Supplementary files.

Table 1. U–Pb data for selected zircons from samples OS-LD1 (granite) and OS-LD10 (lundyite)

	Compositional parameters						Radiogenic isotope ratios					Isotopic age (Ma)					
Sample[†]	$\frac{Th^{‡}}{U}$	$\frac{Pb^{*§}}{Pb_c}$	Pb_c (pg)[§]	$\frac{^{206}Pb^{‖}}{^{204}Pb}$	$\frac{^{207}Pb^{¶}}{^{206}Pb}$	Error (%)**	$\frac{^{207}Pb^{¶}}{^{235}U}$	Error (%)**	$\frac{^{206}Pb^{¶}}{^{238}U}$	Error (%)**	Correlation coefficient	$\frac{^{207}Pb^{¶}}{^{206}Pb}^{††}$	±**	$\frac{^{207}Pb^{††}}{^{235}U}$	±**	$\frac{^{206}Pb^{††}}{^{238}U}$	±**
OS-LD-1																	
608/7	0.214	5	0.89	358.0007	0.046801	1.472	0.057553	1.593	0.008919	0.200	0.645	39.06	35.19	56.82	0.88	57.240	0.114
611/7	0.635	2	1.54	138.5676	0.047271	2.516	0.058217	2.694	0.008932	0.179	0.997	62.94	59.88	57.46	1.50	57.324	0.102
608/5	0.254	5	0.98	350.2003	0.046819	1.153	0.057939	1.244	0.008975	0.133	0.715	39.99	27.55	57.19	0.69	57.600	0.076
608/6	0.399	2	1.63	135.4215	0.051396	4.910	0.082979	5.250	0.01171	0.347	0.980	258.63	112.75	80.94	4.08	75.046	0.259
611/8	0.305	22	1.72	1420.336	0.056662	0.132	0.101743	0.228	0.013023	0.106	0.946	478.42	2.92	98.38	0.21	83.409	0.088
OS-LD-10																	
611/2	0.771	13	1.68	757.4022	0.046715	1.249	0.056102	1.299	0.00871	0.205	0.317	34.68	29.89	55.42	0.70	55.906	0.114
611/1	0.875	12	1.85	702.6069	0.047304	0.607	0.056842	0.676	0.008715	0.074	0.963	64.58	14.45	56.14	0.37	55.938	0.041
608/9	0.994	14	0.88	785.0002	0.047007	0.411	0.056516	0.467	0.00872	0.077	0.800	49.57	9.80	55.82	0.25	55.968	0.043
608/10	0.684	14	0.87	832.9341	0.046787	0.337	0.056265	0.398	0.008722	0.068	0.935	38.36	8.05	55.58	0.22	55.981	0.038
610/15	0.946	16	0.45	859.4617	0.046718	0.629	0.05621	0.691	0.008726	0.085	0.772	34.82	15.06	55.53	0.37	56.009	0.047
608/3	0.764	33	0.57	1882.466	0.04694	0.279	0.056543	0.318	0.008737	0.086	0.566	46.15	6.66	55.85	0.17	56.075	0.048
608/11	0.755	15	1.15	847.0948	0.047127	0.382	0.056783	0.442	0.008739	0.075	0.848	55.66	9.11	56.08	0.24	56.088	0.042
611/4	0.766	9	1.42	531.0457	0.047004	0.704	0.056638	0.768	0.008739	0.108	0.651	49.42	16.79	55.94	0.42	56.092	0.060

The grains used to calculate the ages are shown in bold. [†]611/8, 608/6, etc. represent labels for single zircon grains; all grains were annealed and chemically abraded after Mattinson (2005). [‡]Model Th/U ratio calculated from the radiogenic $^{208}Pb/^{206}Pb$ ratio and $^{207}Pb/^{235}U$ age. [§]Pb* and Pb_c represent radiogenic and common Pb, respectively. Calculated in mol.%. ^{206}Pb* with respect to radiogenic and blank common Pb. [‖]Measured ratio corrected for spike and fractionation only. [¶]Corrected for fractionation, spike and common Pb; All common Pb was assumed to be from the procedural blank: $^{206}Pb/^{204}Pb = 18.07 ±0.30\%$; $^{207}Pb/^{204}Pb = 15.57 ±0.20\%$; $^{208}Pb/^{204}Pb = 37.85 ± 0.30\%$ (all uncertainties 1σ). **Errors are 2σ, propagated using the algorithms of Schmitz and Schoene (2007). [††]Calculations are based on the decay constants of Jaffey *et al.* (1971). $^{206}Pb/^{238}U$ and $^{207}Pb/^{206}Pb$ ages corrected for initial disequilibrium in $^{230}Th/^{238}U$ using Th/U [magma] = 3 ±0.5.

Results

Zircon description and age data

A granite sample from the south of Lundy Island (OS-LD1; Fig. 2) and a lundyite dyke sample from near the pier (OS-LD10) were chosen for dating because both contained abundant zircons after the separation process. The U–Pb ages for selected zircons are presented in Table 1. The cathodoluminescence images suggested the presence of two distinct groups of zircons based on their internal textures. The zircons from granite sample OS-LD1 exhibit pronounced oscillatory zoning with variations in the thickness of the bands (Fig. 3). In addition to the oscillatory zoning observed in most grains (e.g. 608/5; Fig. 3a), resorption–recrystallization textures and overprinting oscillatory zonation can also be observed (e.g. 611/7; Fig. 3c). The zircons from the lundyite sample (OS-LD10) show faint outer zoning and homogeneous inner domains (Fig. 4). Grain 611/4 shows an inner oscillatory zoned domain with a partially resorbed core, overgrown by a faintly oscillatory domain (Fig. 4a).

Five zircons were analysed from the granite sample OS-LD1 (Table 1). The zircons show a spread in dates from 83.409 ± 0.088 to 57.240 ± 0.114 Ma. Three crystals (608/5, 611/7 and 608/7) are concordant, with the youngest two (611/7 and 608/7) overlapping with dates of 57.324 ± 0.102 and 57.240 ± 0.114 Ma, respectively (Fig. 3; Table 1). Eight zircons were analysed from the lundyite

dyke sample (OS-LD10, Table 1). The zircons show a spread in dates from 56.092 ± 0.060 to 55.91 ± 0.11 Ma. Five analyses are equivalent within error and do not show distinct oscillatory growth zones, which give a weighted mean $^{206}Pb/^{238}U$ age of $55.970 \pm 0.021/0.030/0.070$ Ma (MSWD = 1.69; Fig. 4).

Comparison of whole-rock and REE data

Two granite samples (OS-LD2 and OS-LD7), one dolerite dyke sample (OS-LD5) and one lundyite dyke sample (OS-LD10) were analysed for whole-rock geochemistry, along with the four main felsic ash layers (-33, -17, $+13$ and $+19$) from the Fur Formation in Denmark, to assess whether the Lundy complex could be the source of any of these key marker horizons. These data were complemented by geochemical data from previous studies on the Lundy granites and dykes (Stone 1990; Thorpe et al. 1990; Thorpe and Tindle 1992) and the Danish ash layers (Larsen et al. 2003).

Both the analysed granite samples (coarse- and medium- to fine-grained two-mica $\pm$ garnet $\pm$ tourmaline granites) are peraluminous with an aluminium saturation index of 1.5 and S-type granite characteristics (low Na_2O, CaO and Fe_2O_3; low Sr, Zr, La, Ce and Y; and high P; Chappell and White 2001; Frost et al. 2001). The major element data of the lundyite dyke (OS-LD10) shows minor differences from the granites (OS-LD2, OS-LD7), with slightly
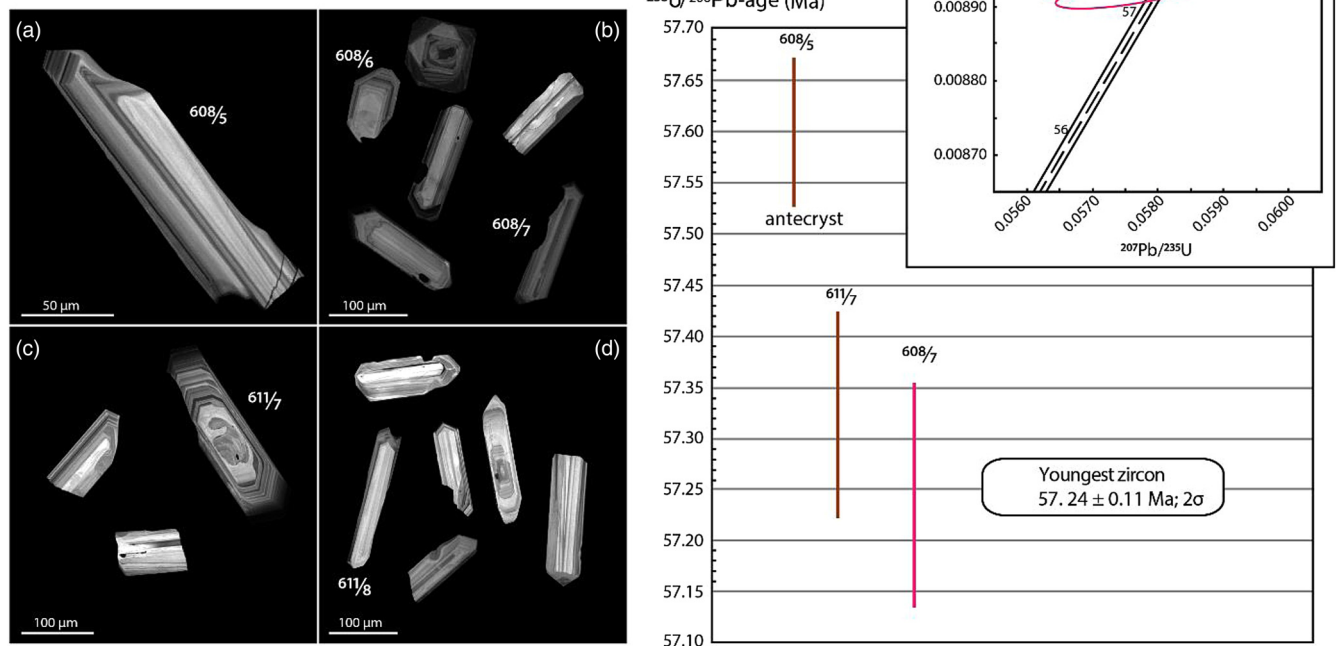
Fig. 3. Left-hand panels: cathodoluminescence images of zircons chosen for dating from granite sample OS-LD1. The numbered grains represent the zircons dated in this study (Table 1). (**a**) A grain with oscillatory and sector-zoning growth zones, broken on one end. (**b**) Grains with growth zones, some with prismatic faces; the grain in the upper left (608/6) has an inner domain with a subrounded shape and featureless texture that, given the discordant $^{207}Pb/^{206}Pb$ date, is interpreted to represent a xenocrystic core. A non-analysed grain at the top left also clearly shows the presence of xenocrystic core material. Grain 608/7 has a rather simple oscillatory zonation with few growth zones. This grain also has the youngest date from this OS-LD1 sample (Table 1). (**c**) The grain in the upper right (611/7) shows a resorption–recrystallization texture and overprinting oscillatory zonation. This analysis is equivalent within uncertainty to 608/7, so this resorption–recrystallization episode is interpreted to have occurred during a late stage in the magma evolution of the granite phase sampled by OS-LD1, probably reflecting the replenishment of new magma with a zircon-undersaturated composition during late-stage crystallization of this magmatic phase. (**d**) Grains with varying textures, such as oscillatory growth zones, resorption–recrystallization textures and core–overgrowth textures. Grain 611/8 is the oldest dated grain in the sample (Table 1). The cathodoluminescence-bright inner domain of this grain is interpreted to represent a xenocrystic (Paleozoic) core with only minor overgrowth during the Paleocene magma entrainment. Right-hand panels: $^{206}Pb/^{238}U$ age diagram for granite sample OS-LD1. The plot shows three out of five analysed zircon grains. The calculated age of the youngest grain is $57.24 \pm 0.11/0.12/0.13$ Ma (2σ, MSWD = 1.20), which is interpreted to best reflect the emplacement age of the Lundy granite. The concordia plot to the upper right of the $^{206}Pb/^{238}U$ age diagram shows the three youngest zircons. All errors are plotted as 2σ.
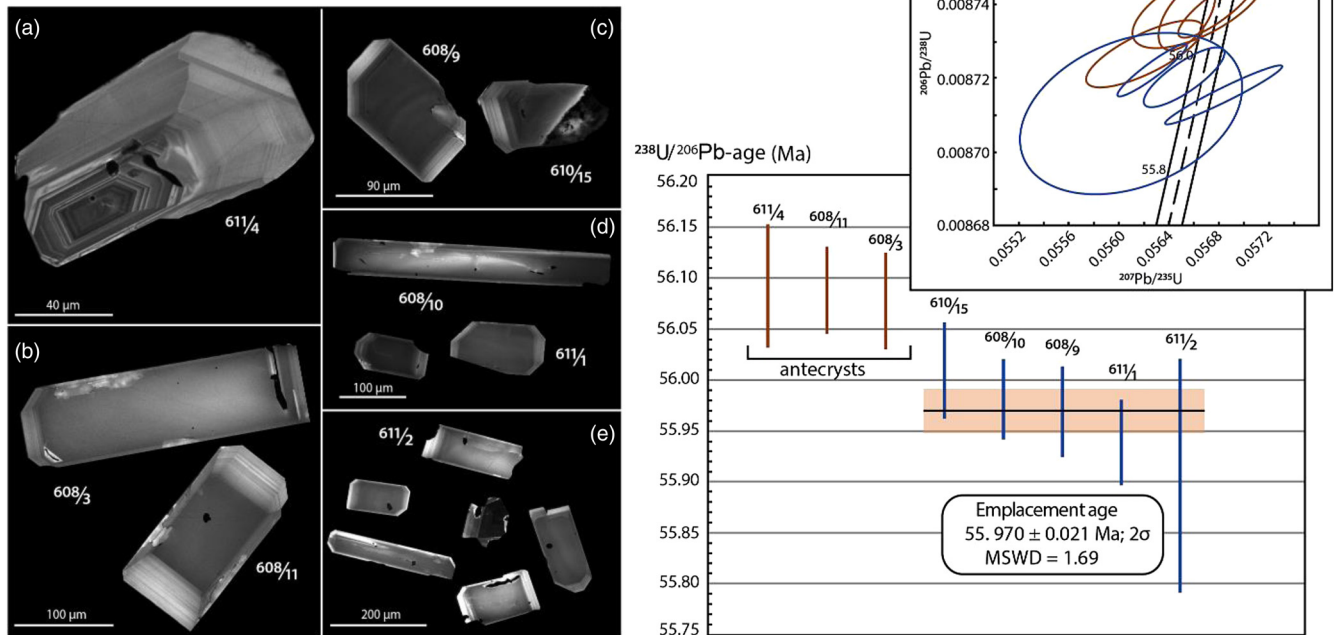
Sample OS-LD10

Fig. 4. Left-hand panels: cathodoluminescence images of zircons chosen for dating from lundyite sample OS-LD10. The numbered grains represent the zircons dated in this study (Table 1). (**a**) Grain 611/4 with an inner oscillatory zoned domain with partially resorbed core, overgrown by a faintly oscillatory domain. This grain is among the older generation of zircons interpreted to represent antecrysts formed early in magma evolution or, alternatively, picked up from host magmatic rocks of the Lundy granite complex. (**b**–**e**) Grains with a homogenous core and faint oscillatory outer zone. Most of these grains (608/9, 608/10, 611/1 and 611/2) were included in the calculation of the mean date that is interpreted to represent emplacement age of the dyke. Each has a simple texture with a homogeneous to faint zonation and one to a few narrow growth zones towards the margins of the grains. Zircon 610/15 (in part c) has several distinct oscillatory growth zones outside the homogeneously zoned interior, comparable with grain 608/11. This may suggest a longer crystallization/magma residence history than the other grains and, although the age is within the uncertainty of the young population (Table 1), it is the oldest of these grains. Given these uncertainties, it is excluded from the mean date calculation. Right-hand panels: $^{206}Pb/^{238}U$ age diagram for lundyite sample OS-LD10. The plot shows the results of all analysed grains from sample OS-LD10, with the weighted mean calculated for the youngest population of zircons (five grains), shown as the black line with the uncertainty as an orange box. The calculated weighted mean is $55.970 \pm 0.021/0.030/0.070$ Ma (MSWD = 1.69), which we interpret to represent the emplacement age of the dyke. It should be noted that we used a correction for Th/U_{magma} of 3 ± 0.5 in this calculation. For a rapidly crystallized rock with a simple fractionation history, the Th/U ratio of the magma may be approximated by the whole-rock composition in the absence of melt inclusion compositional data. In this case, the Th/U ratio of the whole rock is 2.71, within the uncertainty of the Th/U_{magma} estimate used in the calculation. An age using the latter Th/U correction would yield an age 3 kyr younger than that reported here, which is almost identical within uncertainty. For the ease of comparison with other age data, we used a Th/U ratio of 3. The concordia plotted to the upper right of the $^{206}Pb/^{238}U$ age diagram shows all the analysed zircon grains. All errors are plotted as 2σ.

lower SiO_2 (*c.* 69%) and higher Fe_2O_3, MgO and TiO_2 contents (Table 2). On a total alkali v. silica (TAS) classification diagram (Fig. 5), the Lundy complex consists of three distinct populations: (1) the dolerite dykes (OS-LD5; Thorpe and Tindle 1992) plot in the basalt to basaltic andesite fields; (2) an intermediate suite of dykes (Thorpe and Tindle 1992) plot in the trachyte to trachydacite field; and (3) a suite of dykes and the main Lundy granite (OS-LD2 and OS-LD7; Stone 1990; Thorpe *et al.* 1990; Thorpe and Tindle 1992) plot in the rhyolite field. The lundyite sample (OS-LD10) plots just within the rhyolite field between the trachyte dyke and granite populations (Fig. 5). The Danish ash samples from the Fur Formation all plot in the rhyolite field, with ash layers −33, +13 and +19 comparable with the lundyite dyke. Ash layer −17 has very high loss on ignition (LOI) and an extreme TAS classification (Fig. 5).

The Lundy granite samples OS-LD2 and OS-LD7 are rich in Al_2O_3 (*c.* 12.9 wt%) and comparatively poor in CaO (0.4 wt%), Na_2O (*c.* 3.5 wt%) and K_2O (*c.* 4.1 wt%; Table 2), resulting in a peraluminous composition (Fig. 6). This is consistent with previous analyses of the main granite body (Stone 1990; Thorpe *et al.* 1990), confirming a high degree of chemical homogeneity. The lundyite dyke sample (OS-LD10) also plots in the peraluminous field, whereas the dolerite dyke sample (OS-LD5) is metaluminous due to the high CaO content (9.1 wt%; Table 2). These match previous

geochemical studies of Lundy rocks, where the main granite (Stone 1990; Thorpe *et al.* 1990) and cross-cutting trachyte, rhyolite and microgranite dykes (Stone 1990; Thorpe and Tindle 1992) are uniformly peraluminous (Fig. 6). The Lundy complex is therefore unique, within the known extent of the BPIP, with centres such as the Mull, Skye and Slieve Guillon complexes all having peralkaline to metaluminous compositions (Walsh *et al.* 1979; Gamble *et al.* 1992; Aboazoum 1995). On the TAS diagram, the Fur Formation ash layers −33, +13 and +19 plot within the same field as the felsic Lundy suite, whereas ash layer −17 plots as extremely peraluminous, which suggests that extensive alteration has occurred (Fig. 6).

The trace element and REE compositions of the different components of the Lundy igneous complex show comparable signatures to each other (Fig. 7). The REE patterns of the Lundy rocks are flatter relative to other granite suites, both those within the BPIP and local Cornubian batholiths of Permian age (Charles *et al.* 2017). The lundyite dyke (OS-LD10; Fig. 7c, d) shows higher concentrations of the high field strength elements (HFSEs), but similar concentrations of large ion lithophile elements, compared with the Lundy granites (OS-LD2 and OS-LD7; Fig. 7g, h). Other felsic dykes (Fig. 7c, d) show similar, yet unique, REE patterns to both the lundyite and granite samples, indicating that the trachyte and 'low-Zr rhyolites' (the term used by Thorpe and Tindle 1992)

Table 2. Major element (wt%) and trace element (ppm) data for selected rock samples from Lundy (UK) and ash samples from Fur Island (Denmark)

Sample ID	Location	SiO$_2$ (wt%)	Al$_2$O$_3$ (wt%)	Fe$_2$O$_3$ (wt%)	MnO (wt%)	MgO (wt%)	CaO (wt%)	Na$_2$O (wt%)	K$_2$O (wt%)	TiO$_2$ (wt%)	P$_2$O$_5$ (wt%)	LOI	Total
OS-LD2	Lundy	78.5	12.95	1.28	0.04	0.05	0.36	3.65	4.12	0.03	0.05	0.57	101.60
OS-LD5	Lundy	44.4	14.75	14.4	0.26	4.79	9.11	3.65	0.56	3	0.42	2.8	98.14
OS-LD7	Lundy	77.5	12.9	1.56	0.04	0.06	0.45	3.36	4.19	0.05	0.09	0.5	100.7
OS-LD10	Lundy	68.8	15.35	5.02	0.2	0.12	0.08	3.49	4.31	0.37	0.02	3.2	100.96
Ash layer −33	Fur Island	64.42	12.47	3.52	0.023	0.42	0.47	3.18	2.87	0.124	0.44	12.72	100.66
Ash layer −17	Fur Island	69.02	7.21	1.18	0.026	0.22	0.14	1.13	0.65	1.749	0.14	18.54	100.01
Ash layer +13	Fur Island	65.06	13.75	4.04	0.094	0.17	1.25	2.85	3.21	0.397	0.04	9.36	100.22
Ash layer +19	Fur Island	64.87	12.75	4.89	0.174	0.66	1.31	3.73	3.09	0.942	0.14	7.04	99.60

Sample ID	Location	Sc (ppm)	V (ppm)	Cr (ppm)	Co (ppm)	Ni (ppm)	Cu (ppm)	Zn (ppm)	Ga (ppm)	Rb (ppm)	Sr (ppm)	Y (ppm)	Zr (ppm)
OS-LD2	Lundy	8	2	20	0.5	2	1	35	30.4	487	9.7	43	39
OS-LD5	Lundy	33	370	60	44	38	65	115	21.8	22.4	331	42.5	263
OS-LD7	Lundy	7	2	20	0.5	2	1	68	28.2	439	11.3	44.4	72
OS-LD10	Lundy	1	2	10	0.5	1	5	201	36.2	210	11.7	172	1855
Ash layer −33	Fur Island	1	11	20	4	20	20	170	26	139	31	5	44
Ash layer −17	Fur Island	4	20	20	4	40	10	30	15	20	243	14	1855
Ash layer +13	Fur Island	5	22	20	3	20	30	110	24	91	34	52	321
Ash layer +19	Fur Island	5	21	10	1	10	5	160	29	85	292	40.2	633

Sample ID	Location	Nb (ppm)	Cs (ppm)	Ba (ppm)	La (ppm)	Ce (ppm)	Pr (ppm)	Nd (ppm)	Sm (ppm)	Eu (ppm)	Gd (ppm)	Tb (ppm)	Dy (ppm)
OS-LD2	Lundy	57.4	19.1	50.3	9.8	23.6	3.28	13.2	5.74	0.22	7.93	1.67	9.39
OS-LD5	Lundy	16.2	21.1	177.5	16.2	35.8	5.62	27.2	7.74	2.46	9.09	1.41	8.34
OS-LD7	Lundy	50	19.05	52.8	13.1	29.9	4.13	16	6.03	0.34	7.8	1.59	9.45
OS-LD10	Lundy	79.2	1.62	202	49.9	110.5	16.8	72.2	21.5	2.8	27.5	4.7	30.8
Ash layer −33	Fur Island	16	8.5	239	4.5	12.9	1.59	6.3	2.4	0.4	2	0.3	1
Ash layer −17	Fur Island	363	0.5	2121	39.6	69.4	7.17	23	3.8	1.11	2.6	0.5	2.9
Ash layer +13	Fur Island	15	1.3	168	67.3	137	16.4	62.6	12.5	0.61	10.5	1.6	9.8
Ash layer +19	Fur Island	127	0.9	766	96.1	196	23	84.7	15.4	3.58	11.3	1.67	8.56

Sample ID	Location	Ho (ppm)	Er (ppm)	Tm (ppm)	Yb (ppm)	Lu (ppm)	Hf (ppm)	Ta (ppm)	W (ppm)	Tl (ppm)	Pb (ppm)	Th (ppm)	U (ppm)
OS-LD2	Lundy	1.31	2.86	0.34	2.31	0.2	2.8	8.8	61	0.55	12	7.28	4.95
OS-LD5	Lundy	1.53	4.44	0.54	3.74	0.51	6.1	0.6	0.5	0.16	4	1.71	0.66
OS-LD7	Lundy	1.37	3.38	0.39	2.49	0.25	3.6	5.2	6	0.69	17	8.64	6.96
OS-LD10	Lundy	6.19	19.5	2.82	19.75	2.82	38.9	4.8	7	0.05	22	20.1	7.39
Ash layer −33	Fur Island	0.2	0.4	0.07	0.4	0.05	1.9	1.7	2	0.6	25	1.8	4.6
Ash layer −17	Fur Island	0.6	1.6	0.23	1.5	0.23	30.4	31.6	7	0.1	9	38.9	14.8
Ash layer +13	Fur Island	2	5.7	0.82	5.5	0.9	8.3	1.2	1	0.3	25	5.3	2.5
Ash layer +19	Fur Island	1.57	4.3	0.585	3.58	0.537	18.6	8.14	1.2	0.22	12	15.3	4.09

Samples OS-LD2 and OS-LD7 are from the Lundy G1 granite, whereas samples OS-LD5 and OS-LD10 are from cross-cutting dolerite and lundyite dykes, respectively. The Danish ash samples were collected from Stolleklint Beach (ash layers −33 and −17) and Elke Quarry on Fur Island (see Jones *et al.* 2023).

represent their own distinct magmatic events. The same is true of a microgranite dyke (sample G3; Fig. 7g, h) reported by Stone (1990), which is comparable with the granite composition, but with an even more diminished REE content. The dolerite dykes generally have flat trace element and REE patterns, with slight enrichments in Cs, U and Pb relative to pyrolite mantle (Fig. 7e, f).

Eu anomalies are a powerful tracer of magma evolution given the unique ability of Eu among the lanthanides to exist in a divalent form (Eu^{2+}) under reducing conditions. The formula for Eu anomalies (Eu/Eu*) is calculated by chondrite-normalized elemental variations in the formula:

$$Eu/Eu^* = \frac{Eu_{CN}}{(Sm_{CN} \times Gd_{CN})^{0.5}}$$

For some older geochemical data where the Gd contents were not reported, we substituted Tb_{CN} for Gd_{CN} into this formula as a rough approximation (see Supplementary data). These values are given in italic. The dolerite dyke samples (Fig. 7e) show no Eu anomalies, with calculated Eu/Eu* values of 0.90 (this study) and *0.85–1.17* (Thorpe and Tindle 1992). The trachyte dyke sample (Fig. 7c; Thorpe and Tindle 1992) shows no Eu anomaly either (Eu/Eu* = *0.93*). By contrast, the lundyite dyke shows a slight Eu anomaly, with Eu/Eu* values of 0.35 (this study) and *0.33–0.41* (Thorpe and Tindle 1992). The rhyolite dyke sample has a large negative Eu/Eu* anomaly of *0.16* (Fig. 7c; Thorpe and Tindle 1992), as do the microgranite (G3) samples with Eu/Eu* values of *0.08* (Thorpe *et al.* 1990) and 0.10 (Stone 1990). The main granite body also has large Eu anomalies, with Eu/Eu* values of 0.10–0.15 (this study) and *0.11–0.21* (Thorpe *et al.* 1990). This is coupled with large negative anomalies in Ba, Sr and Ti for the evolved Lundy rocks (Fig. 7). The melt source is generally accepted as the primary control on granite magma chemistry (Clemens and Stevens 2012) and, for the Lundy granite complex, this is likely to involve the mixing of variably fractionated granitic magmas from a largely continental crustal source, whereas the dolerite dykes and associated trachytes/rhyolites mainly formed from a mantle source comparable with other BPIP magmatic rocks (Thorpe *et al.* 1990; Thorpe and Tindle 1992; Charles *et al.* 2017).

The four Danish ash samples show contrasting trace element and REE patterns, indicating that they are sourced from a mix of volcanic systems and have experienced varying degrees of element exchange during diagenesis. Ash layer −33 has the most depleted REE signature of all the measured samples, with HREE values only two to three times greater than chondritic values and a Ce/Yb ratio of 32.3 (Fig. 7a; Table 2). Ash layer −33 has a slight Eu anomaly, with calculated Eu/Eu* values between 0.56 (this study) and 0.65 (Larsen *et al.* 2003; Supplementary data). The only Lundy rocks with a similar REE pattern and depletion to ash layer −33 are the microgranites (G3) analysed by Thorpe *et al.* (1990) and Stone (1990). There is a good agreement in the HREE patterns between ash layer −33 and the microgranites, although the Lundy G3 samples are slightly depleted in LREEs and have a larger negative Eu anomaly (Fig. 7g). The close chemical affinity between ash layer −33 and the microgranite continues in the spider diagram (Fig. 7h), with notable deviations including enriched Cs, Rb, Th, Nb and Y, and depleted Ba, Pb, Sr, P and Ti in the microgranites compared with ash layer −33. There is also a reasonable correlation in the REE patterns between the Lundy granite and ash layer −33 (Fig. 7g), albeit that the trace elements are almost universally enriched by up to an order of magnitude in the granite.

Ash layers +13 and +19 display relatively similar REE patterns to each other (Fig. 7a), with the notable exception that ash layer +13 has an Eu anomaly (Eu/Eu* = 0.16) and ash layer +19 does not (Eu/Eu* = 0.83). Ash layers +13 and +19 are enriched in REEs compared with the lundyite and felsic dykes (Fig. 7c), but the slope

is different, with the Lundy rocks being comparatively depleted in LREEs and enriched in HREEs. The felsic Lundy dykes have Ce/Yb values ranging from 5.6 (lundyite OS-LD10) to 10.3 (trachyte LUN61; Thorpe and Tindle 1992), considerably lower than the Ce/Yb ratios of 24.9 for ash layer +13 and 54.8 for ash layer +19 (Table 2). There are also similarities in trace elements between the trachyte, lundyite and rhyolite dykes and ash layers +13 and +19, including marked depletions in Cs, Ba, Sr, P and Ti (Fig. 7d). However, there is notable variance between these datasets, particularly for the HFSEs, such as Th, Nb and Ta. Ash layer −17 is strongly enriched in HFSEs compared with both the other Fur Formation ash layers and the Lundy rocks (Fig. 7b), discounting Lundy as a source.

Discussion

Age of the Lundy igneous complex

The OS-LD1 sample from the Lundy granite gives a U–Pb radiometric age of 57.24 ± 0.11/0.12/0.13 Ma (2σ, MSWD = 1.20; Fig. 3) as recorded by the youngest analysed zircon with a simple zonation texture consisting of a few growth zones (grain 608/7). It contains older discordant zircons dated to *c.* 75 and *c.* 83 Ma (Table 1), but these grains display evidence of xenocrystic cores (Fig. 3). Charles *et al.* (2017) also found xenocrystic cores from Lundy granite zircons, which they suggest is evidence of Early Paleozoic igneous rocks in the unexposed basement beneath the Lundy complex.

Of the three concordant grains, one zircon (608/5) gives a date of 57.600 ± 0.076 Ma that we interpret to be antecrystic, indicating that the magma system feeding the granite emplacement was active for more than 360 kyr. This is supported by zircon textures showing evidence of resorption and recrystallization, and a rather large variation in zonation patterns. The youngest two zircons have overlapping dates, but the older grain (611/7) shows rather complex textures, with an inner domain displaying resorption–recrystallization overgrown by oscillatory zonation, clearly indicating at least a two-stage punctuated growth history. This zircon analysis also has a clearly elevated Th/U ratio compared with zircon 608/7 (Table 1), indicating that it partly crystallized from a melt with a different chemistry from the latter. Zircon 608/7, by contrast, shows a rather simple growth zonation with few longitudinal growth zones. The simple cathodoluminescence texture of zircon 608/7, combined with the Th/U ratio clearly deviating from zircon 611/7 and the youngest date of this population, suggests that 57.24 ± 0.11/0.12/0.13 Ma best represents the emplacement age of the Lundy granite from the available data. However, this does not preclude the presence of younger zircon and hence a younger age of the main Lundy granite.

The timing of the emplacement of the OS-LD10 lundyite dyke can be derived from the population of overlapping dates of the five zircons with equivalent textures, which are also the youngest analysed, giving a mean age of 55.970 ± 0.021/0.030/0.070 Ma (MSWD = 1.69; Fig. 4). The OS-LD10 sample has the highest measured Zr content of any of the Lundy magmatic rocks (1855 ppm), considerably more than the granite samples analysed in this study (39–263 ppm; Table 2). Previous measurements of samples from this dyke (LUN4 and LUN23; Thorpe and Tindle 1992) also measured high Zr concentrations (1643–1654 ppm), comparable with the OS-LD10 sample and greater than the rest of their dataset of Lundy dykes (115–1207 ppm).

If the high Zr content of the OS-LD10 sample is representative of the melt from which the zircons crystallized, then it is likely that zircon saturation was reached early in the crystallization history of the lundyite dyke. Assuming that this dyke cooled rapidly, the very simple growth zonation in the youngest zircon populations suggest
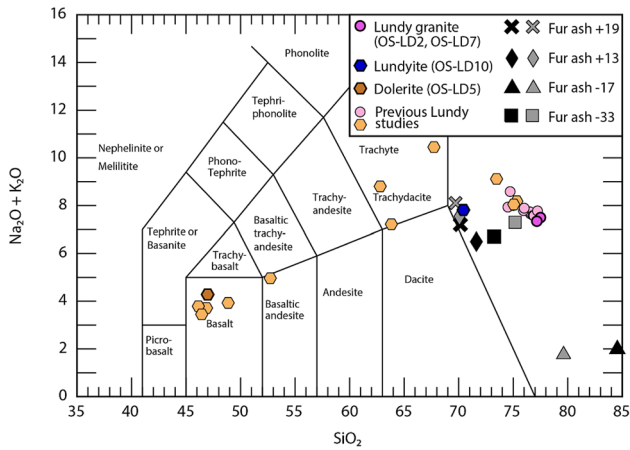
Fig. 5. Total alkali silica diagram for the Lundy Island (UK) and Fur Island (Denmark) samples, normalized to 100%. For the Lundy samples, the circles denote granite samples, whereas the hexagons indicate cross-cutting dykes. Light colours denote geochemical data for the granite (pink) and dyke (orange) samples from previous studies (Stone 1990; Thorpe et al. 1990; Thorpe and Tindle 1992). The Fur Island ash samples are shown by individual black (this study) and grey (Larsen et al. 2003) symbols.

that these crystals grew rapidly from a melt that did not undergo significant fractionation during zircon crystallization, which could indicate that the dyke did not have a prolonged fractionation history from its parental magma. Thorpe and Tindle (1992) suggested that the trachyte and lundyite dykes were formed by fractional crystallization of a basaltic parental melt represented by the Lundy dolerite dykes.

The zircon textures and the *c.* 150 kyr difference between the oldest antecrystic components and the estimated youngest crystallization age suggest that the fractionation history of the parent basaltic melt was short (<200 kyr), as pointed out by Thorpe and Tindle (1992). Bearing in mind the yet unconstrained magma history of the lundyite dykes, the high Zr content and hence the high zircon saturation temperature in the magma could mean that the dyke emplacement was even younger than the age recorded by the
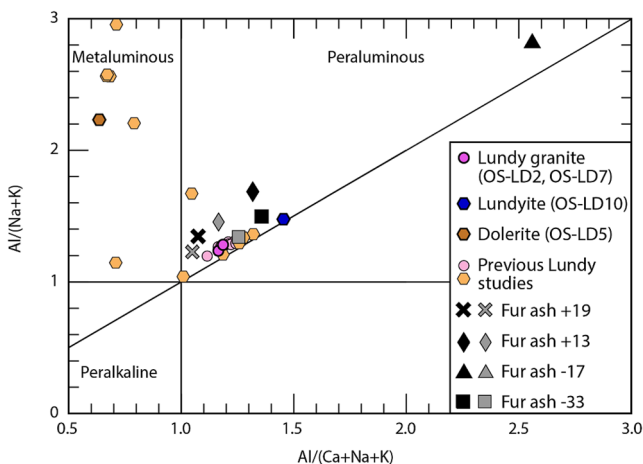
Fig. 6. A/CNK v. A/NK (Al_2O_3/[$Na_2O + K_2O$] v. Al_2O_3/[$CaO + Na_2O + K_2O$]) diagram for the Lundy Island (UK) and Fur Island (Denmark) samples (this study) combined with previous geochemical data for the Lundy dyke (orange) and granite (pink) samples (Stone 1990; Thorpe et al. 1990; Thorpe and Tindle 1992). The granite samples are shown as circles, whereas the dyke samples are denoted by hexagons. The Fur Island ash samples are shown by individual black (this study) and grey (Larsen et al. 2003) symbols.

youngest U–Pb dates presented here. However, because there is no correlation of the individual zircon dates from the youngest zircon population with the width of the oscillatory zoned marginal domains that represent the latest zircon growth, a younger age that is not encompassed by the uncertainty in our preferred age interpretation is unlikely.

The dates determined from this study represent a significant improvement in the precision and accuracy of the age of the Lundy igneous complex. Prior to this study, U–Pb secondary ion mass spectrometry dating by Charles et al. (2017) reported a range of ages for the Lundy granite from 59.8 ± 0.4 to 58.4 ± 0.4 Ma, interpreting this as a two-episode emplacement event (Fig. 8). This study also reported the age of two evolved dykes (Fig. 8). A 'felsite' dyke (LY32) on Lundy's west coast (Fig. 2), which is likely the same as the 'low-Zr' rhyolite dyke LUN69 analysed by Thorpe and Tindle (1992), has an age of 57.3 ± 0.8 Ma. A 'trachyte' dyke (LY13) from near Lundy pier gave an age of 57.2 ± 0.5 Ma (Charles et al. 2017). The LY13 dyke may be the same as the lundyite dyke samples OS-LD10 (this study), and LUN4 and LUN23 (Thorpe and Tindle 1992), because it is the only significant evolved dyke identified near Lundy's pier and may have been identified as trachyte purely on outcrop appearance (Charles et al. 2017), which is similar to that of OS-LD10 (Fig. 2).

If sample LY13 is indeed from the lundyite dyke, then the age of 57.2 ± 0.5 Ma is *c.* 1.24 Myr older than the age determined for OS-LD10. Similarly, the age difference between their youngest granite sample (LY25; Charles et al. 2017) and OS-LD1 is *c.* 1.16 Myr. This suggests that the discrepancy between the ages reported here and Charles et al. (2017) is most likely due to (1) possible age variations within the 91500 zircon standard (Wiedenbeck et al. 2004) and/or (2) possible inaccuracy related to the U/Th content given the measured high U and Th contents of zircons from Charles et al. (2017), which yielded consistently offset ages (White and Ireland 2012). If correct, this would mean that the Lundy granite emplacement is constrained to between *c.* 58.6 and 57.24 Ma (Fig. 8) and that the Lundy igneous complex was active for at least 2.6 Myr.

The refined emplacement ages of the main Lundy granite (57.24 ± 0.11 Ma) and the lundyite dyke (55.970 ± 0.021 Ma) are noteworthy in the wider context of the evolution of the NAIP and the pronounced changes in climate across the Paleocene–Eocene boundary. Incised sedimentary sequences from the Faroe–Shetland basin are evidence of sporadic thermal uplift events, manifest as the onset of a regional marine regression between 58 and 57 Ma, with maximum uplift occurring at *c.* 56 Ma (Shaw Champion et al. 2008; Hartley et al. 2011; Conway-Jones and White 2022). These match the granite emplacement and the lundyite dyke ages, indicating that magmatic activity was elevated during thermal uplift events from the NAIP. The lundyite emplacement age also falls between the two current leading estimates for the onset of the PETM, which are 56.01 ± 0.05 Ma (Zeebe and Lourens 2019) and 55.93 Ma (Westerhold et al. 2017). This suggests that not only was Lundy the most southerly known expression of the NAIP, but it was one of the last remnants of silicic magmatism from the BPIP that was also coeval with the Paleocene–Eocene boundary.

Lundy magmatism as a potential source for Eocene ash layers in Denmark

The Lundy igneous complex is likely to have had a surface volcanic component because the granite was emplaced at shallow crustal depths (1–2 km) within a sinistral extensional regime (Stone 1990; Thorpe et al. 1990; Charles et al. 2017). The rapid emplacement of numerous dolerite, trachyte and rhyolite dykes, coupled with comparisons of outcrops of intrusive and extrusive components from other BPIP centres (e.g. Upton 1988), has been cited as strong
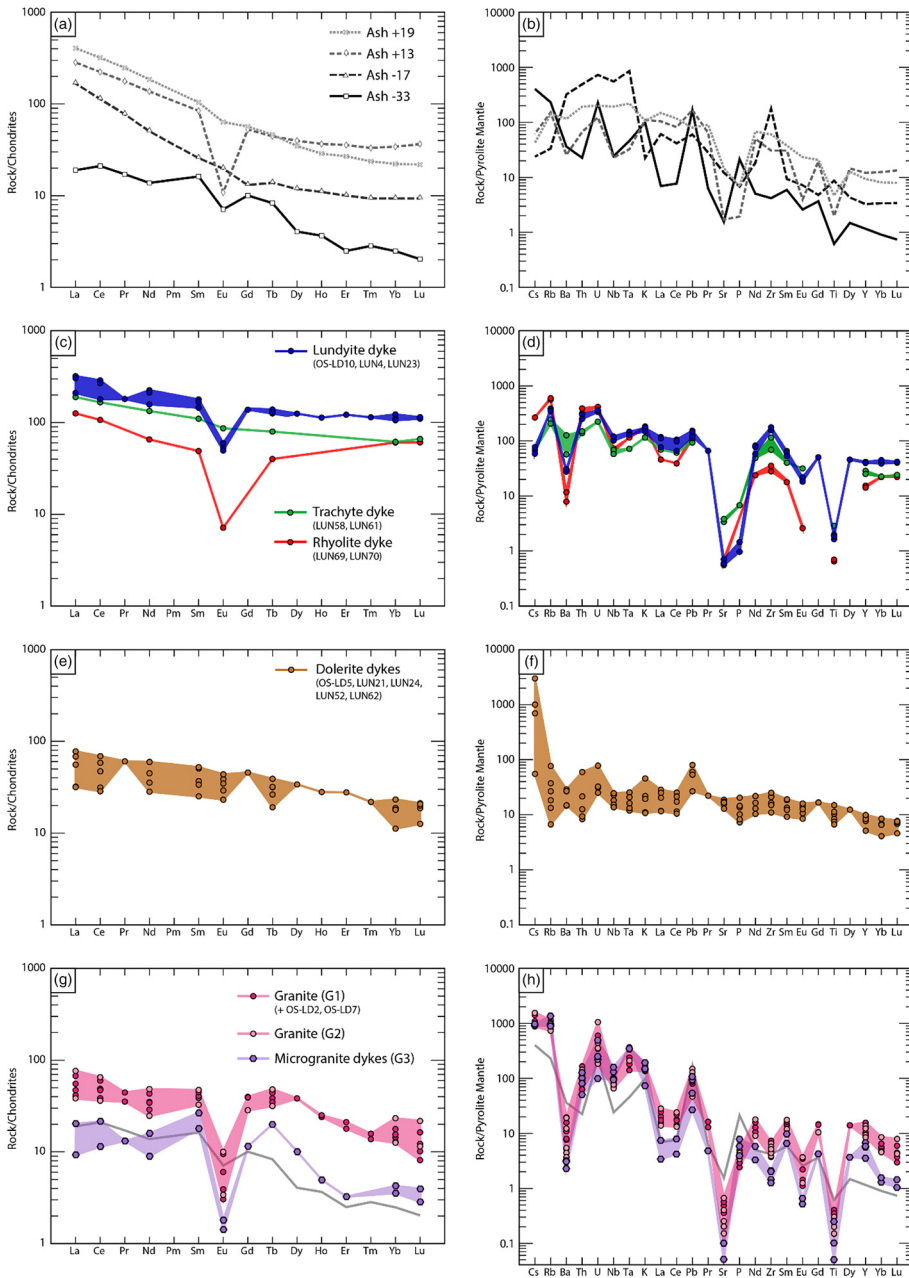
Fig. 7. Rare earth element (left-hand column) and spider (right-hand column) diagrams for selected Lundy Island (UK) and Fur Island (Denmark) samples after Sun and McDonough (1989) and McDonough and Sun (1995), respectively. (**a**, **b**) Ash layers −33, −17, +13 and +19 from the Fur Formation in Denmark (this study). (**c**, **d**) The lundyite (blue; samples OS-LD10, this study, and LUN4 and LUN23, Thorpe and Tindle 1992), trachyte (green; samples LUN58 and LUN61, Thorpe and Tindle 1992) and rhyolite (red; LUN69 and LUN70, Thorpe and Tindle 1992) dykes on Lundy Island. (**e**, **f**) Dolerite dykes (brown) based on sample OS-LD5 (this study) and LUN21, LUN24, LUN52 and LUN62 (Thorpe and Tindle 1992). (**g**, **h**) Granite intrusion (pink), separated into the G1 series labelled with dark pink markers (Thorpe *et al.* 1990; and OS-LD2 and OS-LD7, this study) and G2 series with light pink markers (Thorpe *et al.* 1990). Microgranite samples from the G3 dyke series (Stone 1990; Thorpe *et al.* 1990) are shown in purple. The ash layer −33 data are shown as a grey line for reference.

evidence for the development of a substantial composite volcano above this complex (Thorpe and Tindle 1992). These researchers suggested that evidence of such volcanism should be present in proximal sedimentary systems, but such depocenters close to the NAIP are largely missing due to NAIP uplift instigating a regional unconformity between 57 and 55 Ma (e.g. Conway-Jones and White 2022). This requires investigations further afield and the Fur Formation in Denmark is an ideal locality because the hosting diatomite has resulted in the excellent preservation of volcanic glass and minerals (Stokke *et al.* 2020*b*).

Larsen *et al.* (2003) were the first to undertake a detailed study of these ash layers and proposed a NAIP origin for these ashes based on geochemical evidence, despite all the known volcanic centres estimated to be between 750 and 1500 km from the depositional location of the Fur Formation at that time (Abdelmalak *et al.* 2016). Earlier studies had assumed that these ashes were derived from local sources in the Skagerrak or North Sea (e.g. Pedersen *et al.* 1975), but extensive geophysical and seismic surveys have found no evidence of any Paleogene volcanic centres in this area. The Lundy igneous complex was proposed as a potential source for ash layer −33, and potentially ash layers +13 and +19, based on limited trace

element data (Larsen *et al.* 2003). Here, we use the improved geochronological and geochemical data to revisit this hypothesis.

Ash transport limitations

Lundy Island is currently 1100 km away from Fur Island (Fig. 1) and that distance has not changed significantly in the last 56 Myr. A simple transport model, based on the work of Stevenson *et al.* (2015), was run to determine whether it is feasible for ash to travel such distances (Fig. 9). The model estimates how far a grain of a given diameter travels when released from a given height into wind of given speed. It assumes constant wind speeds at all altitudes and straight-line transport from source to deposition. A 60-μm particle size is assumed based on the measured mean grain size of ash layer −33 particles in the Fur Formation (Lisica 2021). The source code for the modelling can be viewed on GitHub at https://tinyurl.com/LundyAsh.

The model suggests that, for average wind speeds greater than *c.* 8 m s^{-1}, 60-μm rhyolite ash particles erupted to an altitude of 10–25 km can travel the 1100 km from Lundy to Fur Island (Fig. 9). This minimum eruption plume height corresponds to a sub-Plinian
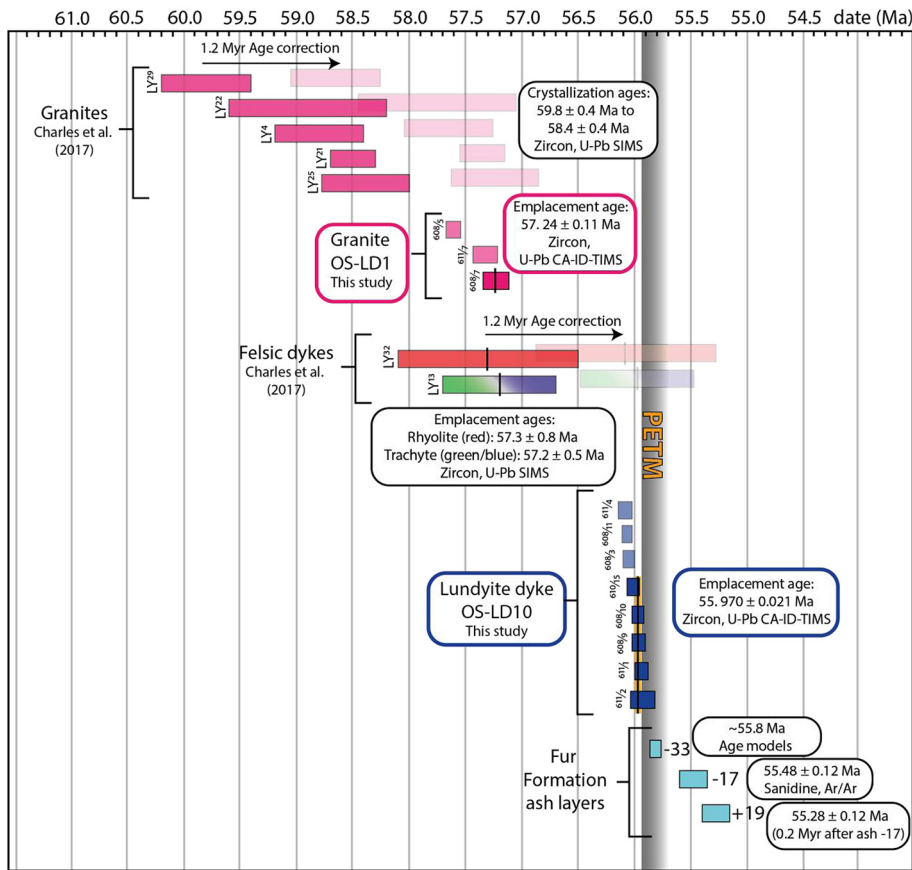
Fig. 8. Synthesis of age data from the Lundy igneous complex and correlation with the timing of the Paleocene–Eocene Thermal Maximum (PETM) and the deposition of felsic ash layers in the Fur Formation in Denmark. Samples OS-LD1 and OS-LD10 are from this study; other granite and felsic dyke ages are from Charles *et al.* (2017). The Lundy granites are shown in pink, the lundyite dyke is shown in blue, the rhyolite LY32 is shown in red and the 'trachyte' sample LY13 is shown in green/blue because it is likely that this is actually the lundyite dyke. The transparent horizontal bars are copies of the Charles *et al.* (2017) dataset and show where these samples would plot if they were corrected to be 1.2 Myr younger to match the emplacement ages of the granite (OS-LD1) and lundyite dyke (OS-LD10). The age of the Danish ash layer −33 is derived from its position within the PETM carbon isotope excursion relative to a dated bentonite during the PETM in Svalbard (Charles *et al.* 2011; Jones *et al.* 2023). Ash layer −17 was dated using Ar/Ar methods (Storey *et al.* 2007a) and the age of ash layer +19 is derived from an estimate of 200 kyr after ash layer −17 based on cyclostratigraphy (Westerhold *et al.* 2009). The onset of the PETM is based on Westerhold *et al.* (2017), but could have begun as early as 56.01 ± 0.05 Ma based on an alternative cyclostratigraphic reconstruction (Zeebe and Lourens 2019).

eruption or larger (VEI 4; erupted volume 1 km^3 dense rock equivalent [DRE]; Cioni *et al.* 2015; Pyle 2015). However, ash layer −33 is *c.* 14 cm thick and normally graded (Jones *et al.* 2019), which is much thicker (and therefore greater in magnitude) than would be expected for a sub-Plinian eruption deposit at this distance. Egger and Brückl (2006) estimated that the thickest silicic ash in the sequence (ash layer +19) was produced by an eruption of 1200 km^3 DRE volume, although this is likely to represent an upper limit because they assumed an equal deposit thickness in all

directions (i.e. circular isopachs). Ash layer +19 is slightly thicker (15–20 cm) than ash layer −33, but it is fair to assume that ash layer −33 was also of large magnitude (>100 km^3 DRE).

Typically, deposits are thickest in the downwind direction and Denmark was likely to be often downwind from the NAIP if the Paleogene atmospheric circulation was broadly similar to that today. However, theoretical physics suggests that Coriolis forces reduce the influence of wind direction on ash dispersal for the most powerful explosive eruptions (Baines and Sparks 2005; Baines *et al.* 2008). In a review of the thickness of ash layers found in deep-sea cores, Mahony *et al.* (2016) concluded that layers >10 cm thick at distances of 1000 km from the source were likely produced by caldera-forming eruptions with VEI >6. Such eruptions have an average recurrence interval of 80 years and correspond to at least 100 km^3 DRE of erupted material (Pyle 2015). This is not exceptional in geological terms and therefore the thickness of these ash horizons is not incompatible with Lundy being the source.

Size of the Lundy granite

Another method for assessing whether the Lundy complex could have generated a large-volume eruption is to estimate the intrusion size. For comparison, the 150 km^3 DRE Campanian Ignimbrite eruption in Italy at *c.* 39 ka resulted in the formation of a 14 km diameter caldera (Marianelli *et al.* 2006). Early estimates of the area of the Lundy granite, based on observed Bouguer anomalies from a land transect on Lundy Island, gave a magma chamber diameter of 4.8 km, a vertical thickness of 1.6 km and a volume of *c.* 30 km^3 (Bott *et al.* 1958). This translates to an area of 18 km^2, *c.* 4.5 times the size of the current area of Lundy Island (4 km^2). However, comprehensive mapping of the Bristol Channel has identified a large, roughly spherical, positive gravity anomaly (peaking at *c.*
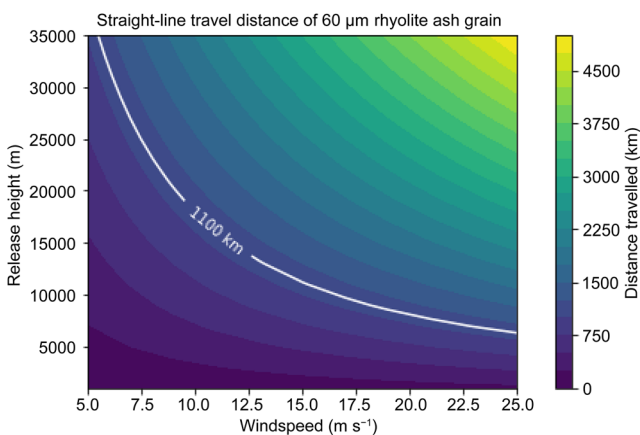
Fig. 9. Ash particle dispersal model after Stevenson *et al.* (2015). The model uses estimates for a 60 μm rhyolitic ash particle and a 1100 km transport distance (shown as the white line). The input parameters use a rhyolitic glass density of 2400 kg m^{-3}, a grain sphericity of 0.7, a size-dependent function (Bonadonna and Phillips 2003) and a Ganser fall velocity model (Ganser 1993).

23 mgal) *c.* 10 km to the WNW of Lundy (Fig. 10; Brooks and Thompson 1973). This positive anomaly matches the features observed beneath other BPIP centres, including Skye, Rum, Mull, Carlingford, Ardnamurchan and Arran (McQuillan and Tuson 1963; Bott and Tuson 1973), and are interpreted to be the result of mafic rocks within the magmatic plumbing system (Brooks and Thompson 1973). By contrast, the Cornubian batholith intrusions, such as Dartmoor, are marked by pronounced negative gravity anomalies (Fig. 10).

The diameters of the exposed BPIP centres range from *c.* 6 km (Ardnamurchan) to *c.* 20 km (Skye), suggesting that the Lundy granite is likely to be in this range. The roughly circular positive gravity anomaly to the west of Lundy has a radius of *c.* 13 km (Fig. 10), which equals an area of *c.* 530 km^2. Even if the granite body is half the diameter of this positive anomaly and the same thickness as calculated by Bott *et al.* (1958), then it would still have an area of 132 km^2 and a volume 210 km^3. This would mean that only a fraction of the complex is currently exposed on Lundy Island and that the system is voluminous enough to have produced large-magnitude eruptions, but detailed investigations are required to constrain the offshore extent of the granite body.

Geochemical and geochronological comparisons

The geochemical data from ash layers need to be treated with caution due to the possible effects of weathering and diagenesis. All four silicic ashes from Fur Island display elevated LOI values (Table 2), with ash layer −17 in particular showing evidence of leaching, a high LOI and major element mobility (Figs 5, 6; Larsen *et al.* 2003), which undermine accurate geochemical comparisons. Although the LOI values for ash layers −33, +13 and +19 are relatively high (Table 2), there are remnants of fresh volcanic glass in ash layer −33 (Larsen *et al.* 2003) and evidence that the diatomite-rich strata in the positive ash series (including ash layers +13 and +19) inhibited the degree of silicate weathering during diagenesis (Stokke *et al.* 2020*b*). Field and laboratory investigations have shown that immobile elements, such as the REEs, are not significantly affected during limited weathering of igneous rocks (Middelburg *et al.* 1988; Hill *et al.* 2000). Previous studies have shown that the geochemical fingerprinting of Paleogene ash horizons with high LOI values using trace elements and REEs is possible (e.g. Jones *et al.* 2016). Ash layers −33, +13 and +19 still retain much of their primary mineral assemblage (Larsen *et al.* 2003), allowing careful comparisons to be made with the Lundy igneous complex.

The geochronological data for the Lundy granite (OS-LD1) indicate that the emplacement age was *c.* 1.44 Myr earlier than the deposition of ash layer −33 (from the currently best available age models of the PETM, where ash layer −33 is located at the end of the PETM body; Charles *et al.* 2011; Jones *et al.* 2023; Fig. 8), so the main granite body can be discounted as a possible source of any Eocene ash layers.

The emplacement age of the lundyite dyke (OS-LD10) suggests that late-stage activity of the Lundy complex continued into the latest Paleocene and it is plausible that activity continued still further into the early Eocene. The magmatism that emplaced the lundyite dyke is also not a source of the four main felsic ash layers in Denmark because the trace element compositions do not match (Fig. 7c, d) and there is a *c.* 140–180 kyr age difference between dyke emplacement and the eruption of ash layer −33 (Fig. 8). There is some geochemical resemblance between the trachyte and rhyolite dykes analysed by Thorpe and Tindle (1992) and ash layers +13 and +19 (Fig. 7c, d), but given the mismatch between dyke emplacement and eruption ages (Fig. 8; Charles *et al.* 2017) and the possible effects of diagenetic overprinting, the sources of these ash layers remain unresolved. Even with the high degree of leaching, the geochemistry of ash layer −17 is completely different from any of the Lundy rocks, confirming that the source volcano is another system, such as that near the Gronau Nunatak in east Greenland (Storey *et al.* 2007*a*; Fig. 1).

There is a close geochemical resemblance between the Lundy microgranite G3 samples (Stone 1990; Thorpe *et al.* 1990) and ash layer −33 in Denmark (Fig. 7g, h). This similarity was first noted by Larsen *et al.* (2003) based on limited geochemical data and our expanded dataset confirms the association. The key areas of variance are large negative anomalies in Eu, Ba and Sr in the microgranites compared with the ash sample (Fig. 7h), suggesting that the microgranites and ash layer −33 originated from a similar parent magma, but that the microgranite had undergone more fractional crystallization of plagioclase prior to emplacement. Comparisons between the G3 microgranite and the host granite body suggest that the diminished REE patterns for the microgranite are indicative of a more evolved melt, likely due to the fractional crystallization of biotite (Stone 1990). The exotic and depleted trace element compositions of ash layer −33 and the G3 microgranites strongly suggests a common parent magma because this REE signature is difficult to replicate through diagenesis. The most likely candidate for the ash layer −33 eruption during the PETM δ^{13}C excursion is therefore the parent magma of the G3 microgranites within the Lundy igneous complex.

Unfortunately, the G3 microgranite outcrops are poorly constrained due to vague locality information in previous studies (Dollar 1941; Stone 1990) and they are very hard to identify because they are only visible in steep-sided cliffs and are very similar in appearance to the host granite, such that they are nearly invisible several metres from the outcrop (Dollar 1941). They are described as mainly thin sheets/dykes only 2–20 cm thick (Stone 1990), which is not indicative of a large volcanic event, such as a caldera collapse. Detailed field investigations are required to understand the field relations between the G3 microgranites and the host rocks, which was beyond the scope of this study given the limitations imposed by the COVID-19 pandemic. Further work needs to be carried out to constrain the geochronology and outcrop extent of Lundy's late-
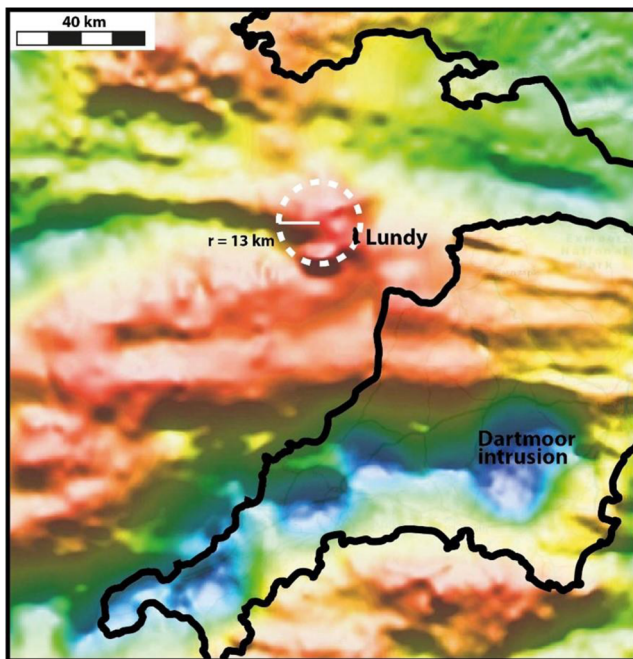
Fig. 10. Gravity anomaly map of the southwestern region of the UK, covering Devon, Cornwall, the Bristol Channel and South Wales. The positive Bouguer anomaly to the west of Lundy Island is shown within a white dashed line. Source: contains British Geological Survey materials © UKRI 2023.

stage magmatic activity to constrain the microgranites within the Lundy igneous complex.

Conclusions

The Lundy igneous complex represents the southernmost known magmatic activity of the NAIP. Its mineralogy and peraluminous S-type geochemical affinity is unique in the BPIP, which has led to the hypothesis that eruptions from a Lundy volcanic centre may be the source of distinctive felsic ash layers (e.g. ash layers −33, +13 and +19) found in the Fur Formation in Denmark, which were deposited during and after the PETM. We present new, high-precision U–Pb ages of $57.24 \pm 0.11/0.12/0.13$ Ma for the main granite body and $55.961 \pm 0.023/0.040/0.070$ Ma for the lundyite dyke, which are significantly younger than the previous age estimations for Lundy rocks. These two ages are notable in that the granite emplacement is broadly coeval with the onset of regional uplift associated with the NAIP, whereas the lundyite dyke occurred during maximum uplift and is within current estimates for the Paleocene–Eocene boundary and the onset of the PETM. The data show that the Lundy complex was active for at least 1.28 Myr, possibly longer, given the presence of antecrystic zircon and previous age estimations (e.g. sample LY29; Charles *et al.* 2017).

New high-resolution major and trace element data for a suite of Lundy rocks and key felsic ash layers from the Fur Formation show that the main granite body and cross-cutting dolerite, trachyte, lundyite and rhyolite dykes share some chemical affinities with ash layers −33, +13 and +19, but REE variations and geochronological differences indicate that none of these samples was the source of the ash layers in Denmark. By contrast, there is a close chemical affinity between thin microgranite dykes within the Lundy complex and ash layer −33, suggesting that late-stage magmatic activity at Lundy could indeed be the source of this key marker horizon within the PETM. This would require the Lundy complex to have remained active for *c.* 140–180 kyr beyond the intrusion of the lundyite dyke (*c.* 55.8 Ma; Jones *et al.* 2023). Considerations of ash transport limitations and magma chamber dimensions suggest that a large-magnitude (>VEI 6, >100 km^3 DRE) caldera-forming event is required to produce a 14 cm thick deposit (ash layer −33) over 1100 km from the source. The offshore extent of the Lundy complex is currently poorly constrained, but gravity anomalies suggest that the magmatic plumbing system is of sufficient magnitude to produce such an eruption. Further work is required to constrain the emplacement age and outcrop extent of the late-stage microgranites to confirm whether this could represent an early Eocene eruption from the Lundy complex.

Scientific editing by Martin Whitehouse

Author contributions **KL**: conceptualization (equal), formal analysis (equal), writing – original draft (equal), writing – review and editing (equal); **LEA**: formal analysis (equal), writing – original draft (equal), writing – review and editing (equal); **JAS**: formal analysis (supporting); **DAJ**: writing – original draft (supporting); **AB-B**: writing – original draft (supporting); **MTJ**: conceptualization (equal), data curation (equal), writing – original draft (supporting), writing – review and editing (equal).

Competing interests The authors declare that they have no known competing financial interests or personal relationships that could have appeared to influence the work reported in this paper.

Data availability All the data and figures in their original files are available as repository material at https://github.com/karloli/Lundy

References

Abdelmalak, M.M., Planke, S., Faleide, J.I., Jerram, D.A., Zastrozhnov, D., Eide, S. and Myklebust, R. 2016. The development of volcanic sequences at rifted margins: new insights from the structure and morphology of the Vøring Escarpment, mid-Norwegian margin. *Journal of Geophysical Research: Solid Earth*, **121**, 5212–5236, https://doi.org/10.1002/2015JB012788

Abdelmalak, M.M., Planke, S. *et al.* 2019. Breakup volcanism and plate tectonics in the NW Atlantic. *Tectonophysics*, **760**, 267–296, https://doi.org/10.1016/j.tecto.2018.08.002

Aboazoum, A.S.A. 1995. *Petrogenesis of Palaeocene Granites, Island of Skye, NW Scotland*. PhD thesis, University of Glasgow.

Anderson, H. 2013. *The Origin and Nature of Cenozoic Faulting in North-East Ireland and the Irish Sea*. PhD thesis, University College Dublin.

Anderson, H., Walsh, J.J. and Cooper, M.R. 2018. The development of a regional-scale intraplate strike-slip fault system; Alpine deformation in the north of Ireland. *Journal of Structural Geology*, **116**, 47–63, https://doi.org/10.1016/j.jsg.2018.07.002

Baines, P.G. and Sparks, R.S.J. 2005. Dynamics of giant volcanic ash clouds from supervolcanic eruptions. *Geophysical Research Letters*, **32**, L24808, https://doi.org/10.1029/2005GL024597

Baines, P.G., Jones, M.T. and Sparks, R.S.J. 2008. The variation of large-magnitude volcanic ash cloud formation with source latitude. *Journal of Geophysical Research*, **113**, D21204, https://doi.org/10.1029/2007JD009568

Bøggild, O.B. 1918. Den vulkanske aske i moleret samt en oversigt over Danmarks ældre Tertierbjergarter. Tekst. *Danmarks Geologiske Undersøgelse II. Række*, **33**, 1–159, https://doi.org/10.34194/raekke2.v33.6818

Bonadonna, C. and Phillips, J.C. 2003. Sedimentation from strong volcanic plumes. *Journal of Geophysical Research: Solid Earth*, **108**, https://doi.org/10.1029/2002JB002034

Bott, M.H.P. and Tuson, J. 1973. Deep structure beneath the Tertiary volcanic regions of Skye, Mull and Ardnamurchan, north-west Scotland. *Nature Physical Science*, **242**, 114–116, https://doi.org/10.1038/physci242114a0

Bott, M.H.P., Day, A.A. and Masson-Smith, D. 1958. The geological interpretation of gravity and magnetic surveys in Devon and Cornwall. *Philosophical Transactions of the Royal Society of London. Series A, Mathematical and Physical Sciences*, **251**, 161–191, https://doi.org/10.1098/rsta.1958.0013

Bowring, J.F., McLean, N.M. and Bowring, S.A. 2011. Engineering cyber infrastructure for U–Pb geochronology: Tripoli and U–Pb Redux. *Geochemistry, Geophysics, Geosystems*, **12**, https://doi.org/10.1029/2010GC003479

Brooks, M.J. and Thompson, M.S. 1973. The geological interpretation of a gravity survey of the Bristol Channel. *Journal of the Geological Society, London*, **129**, 245–274, https://doi.org/10.1144/gsjgs.129.3.0245

Bryan, S.E. and Ernst, R.E. 2008. Revised definition of large igneous provinces (LIPs). *Earth-Science Reviews*, **86**, 175–202, https://doi.org/10.1016/j.earscirev.2007.08.008

Chambers, L.M., Pringle, M.S. and Parrish, R.R. 2005. Rapid formation of the Small Isles Tertiary centre constrained by precise ^{40}Ar/^{39}Ar and U–Pb ages. *Lithos*, **79**, 367–384, https://doi.org/10.1016/j.lithos.2004.09.008

Chappell, B.W. and White, A.J. 2001. Two contrasting granite types: 25 years later. *Australian Journal of Earth Sciences*, **48**, 489–499, https://doi.org/10.1046/j.1440-0952.2001.00882.x

Charles, A.J., Condon, D.J. *et al.* 2011. Constraints on the numerical age of the Paleocene–Eocene boundary. *Geochemistry, Geophysics, Geosystems*, **12**, https://doi.org/10.1029/2010GC003426

Charles, J.H., Whitehouse, M.J., Andersen, J.Ø., Shail, R.K. and Searle, M.P. 2017. Age and petrogenesis of the Lundy granite: Paleocene intraplate peraluminous magmatism in the Bristol Channel, UK. *Journal of the Geological Society, London*, **175**, 44–59, https://doi.org/10.1144/jgs2017-023

Cioni, R., Pistolesi, M. and Rosi, M. 2015. Plinian and subplinian eruptions. *In:* Sigurdsson, H. (ed.) *The Encyclopedia of Volcanoes*. Academic Press, 519–535, https://doi.org/10.1016/B978-0-12-385938-9.00029-8

Clemens, J.D. and Stevens, G. 2012. What controls chemical variation in granitic magmas? *Lithos*, **134**, 317–329, https://doi.org/10.1016/j.lithos.2012.01.001

Condon, D.J., Schoene, B., McLean, N.M., Bowring, S.A. and Parrish, R.R. 2015. Metrology and traceability of U–Pb isotope dilution geochronology (EARTHTIME Tracer Calibration Part I). *Geochimica et Cosmochimica Acta*, **164**, 464–480, https://doi.org/10.1016/j.gca.2015.05.026

Conway-Jones, B.W. and White, N. 2022. Paleogene buried landscapes and climatic aberrations triggered by mantle plume activity. *Earth and Planetary Science Letters*, **593**, 117644, https://doi.org/10.1016/j.epsl.2022.117644

Cooper, M.R., Anderson, H., Walsh, J.J., Van Dam, C.L., Young, M.E., Earls, G. and Walker, A. 2012. Palaeogene Alpine tectonics and Icelandic plume-related magmatism and deformation in Northern Ireland. *Journal of the Geological Society, London*, **169**, 29–36, https://doi.org/10.1144/0016-76492010-182

Cramer, B.S., Toggweiler, J.R., Wright, J.D., Katz, M.E. and Miller, K.G. 2009. Ocean overturning since the Late Cretaceous: inferences from a new benthic foraminiferal isotope compilation. *Paleoceanography*, **24**, https://doi.org/10.1029/2008PA001683

Dollar, A.T.J. 1941. The Lundy complex: its petrology and tectonics. *Quarterly Journal of the Geological Society, London*, **97**, 39–77, https://doi.org/10.1144/GSL.JGS.1941.097.01-04.03

Drake, S.M., Brown, D. *et al.* 2022. Catastrophic caldera-forming eruptions and climate perturbations: the result of tectonic and magmatic controls on the Paleocene–Eocene Kilchrist Caldera, Isle of Skye, NW Scotland. *Volcanica*, **5**, 397–432, https://doi.org/10.30909/vol.05.02.397432

Edmonds, E.A., Williams, B.J. and Taylor, R.T. 1979. *Geology of Bideford and Lundy Island: memoir for 1:50 000 geological sheet 292, new series, with sheets 275, 276, 291 and part of sheet 308*. HMSO.

Egger, H. and Brückl, E. 2006. Gigantic volcanic eruptions and climatic change in the early Eocene. *International Journal of Earth Sciences*, **95**, 1065–1070, https://doi.org/10.1007/s00531-006-0085-7

Emeleus, C.H., Bell, B.R. and Stephenson, D. 2005. *The Palaeogene Volcanic Districts of Scotland*. Vol. 3. British Geological Survey.

Frost, B.R., Barnes, C.G., Collins, W.J., Arculus, R.J., Ellis, D.J. and Frost, C.D. 2001. A geochemical classification for granitic rocks. *Journal of Petrology*, **42**, 2033–2048, https://doi.org/10.1093/petrology/42.11.2033

Gamble, J.A., Meighan, I.G. and McCormick, A.G. 1992. The petrogenesis of Tertiary microgranites and granophyres from the Slieve Gullion Central Complex, NE Ireland. *Journal of the Geological Society, London*, **149**, 93–106, https://doi.org/10.1144/gsjgs.149.1.0093

Gamble, J.A., Wysoczanski, R.J. and Meighan, I.G. 1999. Constraints on the age of the British Tertiary Volcanic Province from ion microprobe U–Pb (SHRIMP) ages for acid igneous rocks from NE Ireland. *Journal of the Geological Society, London*, **156**, 291–299, https://doi.org/10.1144/gsjgs.156.2.0291

Ganerød, M., Smethurst, M.A. *et al.* 2010. The North Atlantic Igneous Province reconstructed and its relation to the plume generation zone: the Antrim Lava Group revisited. *Geophysical Journal International*, **182**, 183–202, https://doi.org/10.1111/j.1365-246X.2010.04620.x

Ganerød, M., Chew, D.M., Smethurst, M.A., Troll, V.R., Corfu, F., Meade, F. and Prestvik, T. 2011. Geochronology of the Tardree rhyolite complex, Northern Ireland; implications for zircon fission-track studies, the North Atlantic Igneous Province and the age of the Fish Canyon sanidine standard. *Chemical Geology*, **286**, 222–228, https://doi.org/10.1016/j.chemgeo.2011.05.007

Ganser, G.H. 1993. A rational approach to drag prediction of spherical and nonspherical particles. *Powder Technology*, **77**, 143–152, https://doi.org/10.1016/0032-5910(93)80051-B

Golonka, J. 2009. Phanerozoic paleoenvironment and paleolithofacies maps: Cenozoic. *Geologia/Akademia Górniczo-Hutnicza im Stanisława Staszica w Krakowie*, **35**, 507–587, https://bibliotekanauki.pl/articles/183799

Hall, T.C. 1915. *Note on an Unique Orthophyre of Lundy Which He Proposed to Call 'Lundyite'*. Summary of the Progress of the Geological Society of Great Britain. Geological Survey of Great Britain.

Hamilton, M.A., Pearson, D.G., Thompson, R.N., Kelley, S.P. and Emeleus, C.H. 1998. Rapid eruption of Skye lavas inferred from precise U–Pb and Ar–Ar dating of the Rum and Cuillin plutonic complexes. *Nature*, **394**, 260–263, https://doi.org/10.1038/28361

Hartley, R.A., Roberts, G.G., White, N. and Richardson, C. 2011. Transient convective uplift of an ancient buried landscape. *Nature Geoscience*, **4**, 562–565, https://doi.org/10.1038/ngeo1191

Heilmann-Clausen, C., Nielsen, O.B. and Gersner, F. 1985. Lithostratigraphy and depositional environments in the Upper Paleocene and Eocene of Denmark. *Bulletin of the Geological Society of Denmark*, **33**, 287–323, https://doi.org/10.37570/bgsd-1984-33-26

Heister, L.E., O'Day, P.A., Brooks, C.K., Neuhoff, P.S. and Bird, D.K. 2001. Pyroclastic deposits within the East Greenland Tertiary flood basalts. *Journal of the Geological Society, London*, **158**, 269–284, https://doi.org/10.1144/jgs.158.2.269

Hill, I.G., Worden, R.H. and Meighan, I.G. 2000. Yttrium: the immobility–mobility transition during basaltic weathering. *Geology*, **28**, 923–926, https://doi.org/10.1130/0091-7613(2000)28<923:YTITDB>2.0.CO;2

Horni, J.Á., Hopper, J.R. *et al.* 2017. Regional distribution of volcanism within the North Atlantic Igneous Province. *Geological Society, London, Special Publications*, **447**, 105–125, https://doi.org/10.1144/SP447.18

Hovikoski, J., Fyhn, M.B.W. *et al.* 2021. Paleocene–Eocene volcanic segmentation of the Norwegian–Greenland seaway reorganized high-latitude ocean circulation. *Communications Earth & Environment*, **2**, 172, https://doi.org/10.1038/s43247-021-00249-w

Huyskens, M.H., Zink, S. and Amelin, Y. 2016. Evaluation of temperature–time conditions for the chemical abrasion treatment of single zircons for U–Pb geochronology. *Chemical Geology*, **438**, 25–35, https://doi.org/10.1016/j.chemgeo.2016.05.013

Jaffey, A.H., Flynn, K.F., Glendenin, L.E., Bentley, W.T. and Essling, A.M. 1971. Precision measurement of half-lives and specific activities of ^{235}U and ^{238}U. *Physical Review C*, **4**, 1889, https://doi.org/10.1103/PhysRevC.4.1889

Jerram, D.A. and Widdowson, M. 2005. The anatomy of continental flood basalt provinces: geological constraints on the processes and products of flood volcanism. *Lithos*, **79**, 385–405, https://doi.org/10.1016/j.lithos.2004.09.009

Jolley, D.W., Millett, J.M., Schofield, N. and Broadley, L. 2021. Stratigraphy of volcanic rock successions of the North Atlantic rifted margin: the offshore record of the Faroe–Shetland and Rockall basins. *Earth and Environmental Science Transactions of the Royal Society of Edinburgh*, **112**, 61–88, https://doi.org/10.1017/S1755691021000037

Jones, M.T., Eliassen, G.T. *et al.* 2016. Palaeocene magmatism and rifting events in the North Atlantic–Arctic oceans constrained by geochemistry of bentonites from Svalbard. *Journal of Volcanology and Geothermal Research*, **327**, 571–584, https://doi.org/10.1016/j.jvolgeores.2016.09.014

Jones, M.T., Percival, L.M. *et al.* 2019. Mercury anomalies across the Palaeocene–Eocene thermal maximum. *Climate of the Past*, **15**, 217–236, https://doi.org/10.5194/cp-15-217-2019

Jones, M.T., Stokke, E.W. *et al.* 2023. Tracing North Atlantic volcanism and seaway connectivity across the Paleocene–Eocene Thermal Maximum (PETM). *Climate of the Past*, **19**, 1623–1652, https://doi.org/10.5194/cp-19-1623-2023

King, C. 2016. *A Revised Correlation of Tertiary Rocks in the British Isles and Adjacent Areas of NW Europe*. Geological Society.

Krogh, T.E. 1973. A low-contamination method for hydrothermal decomposition of zircon and extraction of U and Pb for isotopic age determinations. *Geochimica et Cosmochimica Acta*, **37**, 485–494, https://doi.org/10.1016/0016-7037(73)90213-5

Kuiper, K., Deino, A., Hilgen, F., Krijgsman, W., Renne, P. and Wijbrans, J. 2008. Synchronizing rock clocks of Earth history. *Science*, **320**, 500–504, https://doi.org/10.1126/science.1154339

Larsen, L.M., Fitton, J.G. and Pedersen, A.K. 2003. Paleogene volcanic ash layers in the Danish Basin: compositions and source areas in the North Atlantic Igneous Province. *Lithos*, **71**, 47–80, https://doi.org/10.1016/j.lithos.2003.07.001

Larsen, L.M., Pedersen, A.K., Tegner, C., Duncan, R.A., Hald, N. and Larsen, J.G. 2016. Age of Tertiary volcanic rocks on the West Greenland continental margin: volcanic evolution and event correlation to other parts of the North Atlantic Igneous Province. *Geological Magazine*, **153**, 487–511, https://doi.org/10.1017/S0016756815000515

Lisica, K. 2021. *Petrological and Geochronological Investigation of the Lundy Granite and Its Role in the North Atlantic Igneous Province (NAIP)*. Master's thesis, University of Oslo.

Littler, K., Röhl, U., Westerhold, T. and Zachos, J.C. 2014. A high-resolution benthic stable-isotope record for the South Atlantic: implications for orbital-scale changes in Late Paleocene–Early Eocene climate and carbon cycling. *Earth and Planetary Science Letters*, **401**, 18–30, https://doi.org/10.1016/j.epsl.2014.05.054

Ludwig, K.R. 2012. *User's Manual for Isoplot 3.75, A Geochronological Toolkit for Microsoft Excel*. Berkeley Geochronology Center Special Publication, **5**.

Mahony, S.H., Sparks, R.S.J. *et al.* 2016. Increased rates of large-magnitude explosive eruptions in Japan in the late Neogene and Quaternary. *Geochemistry, Geophysics, Geosystems*, **17**, 2467–2479, https://doi.org/10.1002/2016GC006362

Marianelli, P., Sbrana, A. and Proto, M. 2006. Magma chamber of the Campi Flegrei supervolcano at the time of eruption of the Campanian Ignimbrite. *Geology*, **34**, 937–940, https://doi.org/10.1130/G22807A.1

Mattinson, J.M. 2005. Zircon U–Pb chemical abrasion ("CA-TIMS") method: combined annealing and multi-step partial dissolution analysis for improved precision and accuracy of zircon ages. *Chemical Geology*, **220**, 47–66, https://doi.org/10.1016/j.chemgeo.2005.03.011

McDonough, W.F. and Sun, S.-S. 1995. The composition of the Earth. *Chemical Geology*, **120**, 228, https://doi.org/10.1016/0009-2541(94)00140-4

McQuillan, R. and Tuson, J. 1963. Gravity measurements over the Rhum Tertiary plutonic complex. *Nature*, **199**, 1276–1277, https://doi.org/10.1038/1991276a0

Middelburg, J.J., van der Weijden, C.H. and Woittiez, J.R.W. 1988. Chemical processes affecting the mobility of major, minor and trace elements during weathering of granitic rocks. *Chemical Geology*, **68**, 253–273, https://doi.org/10.1016/0009-2541(88)90025-3

Morton, A.C. and Knox, R.O.B. 1990. Geochemistry of late Palaeocene and early Eocene tephras from the North Sea Basin. *Journal of the Geological Society, London*, **147**, 425–437, https://doi.org/10.1144/gsjgs.147.3.0425

Pedersen, A.K., Engell, J. and Rønsbo, J.G. 1975. Early Tertiary volcanism in the Skagerrak: New chemical evidence from ash-layers in the mo-clay of northern Denmark. *Lithos*, **8**, 255–268, https://doi.org/10.1016/0024-4937(75)90009-2

Pyle, D.M. 2015. Sizes of volcanic eruptions. *In:* Sigurdsson, H. (ed.) *The Encyclopedia of Volcanoes*. Academic Press, 257–264, https://doi.org/10.1016/B978-0-12-385938-9.00013-4

Roberts, C.L. and Smith, S.G. 1994. A new magnetic survey of Lundy Island, Bristol Channel. *Proceedings of the Ussher Society*, **8**, 293–293.

Saunders, A.D., Fitton, J.G., Kerr, A.C., Norry, M.J., Kent, R.W., Mahoney, J.J. and Coffin, M.F. 1997. The North Atlantic Igneous Province. *American Geophysical Union, Geophysical Monographs*, **100**, 45–94.

Schmitz, M.D. and Schoene, B. 2007. Derivation of isotope ratios, errors, and error correlations for U–Pb geochronology using ^{205}Pb–^{235}U–(^{233}U)-spiked isotope dilution thermal ionization mass spectrometric data. *Geochemistry, Geophysics, Geosystems*, **8**, https://doi.org/10.1029/2006GC001492

Shaw Champion, M.E., White, N.J., Jones, S.M. and Lovell, J.P.B. 2008. Quantifying transient mantle convective uplift: an example from the Faroe-Shetland basin. *Tectonics*, **27**, TC1002, https://doi.org/10.1029/2007TC002106

Speijer, R.P., Pälike, H., Hollis, C.J., Hooker, J.J. and Ogg, J.G. 2020. The Paleogene Period. *In:* Gradstein, F.M., Ogg, J.G., Schmitz, M.D. and Ogg, G.M. (eds) *Geologic Time Scale 2020*. Elsevier, 1087–1140, https://doi.org/10.1016/B978-0-12-824360-2.00028-0

Stevenson, J.A., Millington, S.C., Beckett, F.M., Swindles, G.T. and Thordarson, T. 2015. Big grains go far: understanding the discrepancy between tephrochronology and satellite infrared measurements of volcanic ash. *Atmospheric Measurement Techniques*, **8**, 2069–2091, https://doi.org/10.5194/amt-8-2069-2015

Stokke, E.W., Jones, M.T., Tierney, J.E., Svensen, H.H. and Whiteside, J.H. 2020*a*. Temperature changes across the Paleocene–Eocene Thermal Maximum – a new high-resolution TEX86 temperature record from the eastern North Sea Basin. *Earth and Planetary Science Letters*, **544**, 116388, https://doi.org/10.1016/j.epsl.2020.116388

Stokke, E.W., Liu, E. and Jones, M.T. 2020*b*. Evidence of explosive hydromagmatic eruptions during the emplacement of the North Atlantic Igneous Province. *Volcanica*, **3**, 227–250, https://doi.org/10.30909/vol.03.02.227250

Stokke, E.W., Jones, M.T., Riber, L., Haflidason, H., Midtkandal, I., Schultz, B.P. and Svensen, H.H. 2021. Rapid and sustained environmental responses to global warming: the Paleocene–Eocene Thermal Maximum in the eastern North Sea. *Climate of the Past*, **17**, 1989–2013, https://doi.org/10.5194/cp-17-1989-2021

Stone, M. 1990. The Lundy granite: a geochemical and petrogenetic comparison with Hercynian and Tertiary granites. *Mineralogical Magazine*, **54**, 431–446, https://doi:10.1180/minmag.1990.054.376.09

Storey, M., Duncan, R.A. and Swisher, C.C. 2007*a*. Paleocene–Eocene thermal maximum and the opening of the northeast Atlantic. *Science*, **316**, 587–589, https://doi.org/10.1126/science.1135274

Storey, M., Duncan, R.A. and Tegner, C. 2007*b*. Timing and duration of volcanism in the North Atlantic Igneous Province: implications for geodynamics and links to the Iceland hotspot. *Chemical Geology*, **241**, 264–281, https://doi.org/10.1016/j.chemgeo.2007.01.016

Sun, S.S. and McDonough, W.F. 1989. Chemical and isotopic systematics of oceanic basalts: implications for mantle composition and processes. *Geological Society, London, Special Publications*, **42**, 313–345, https://doi.org/10.1144/GSL.SP.1989.042.01.19

Thorpe, R.S. and Tindle, A.G. 1992. Petrology and petrogenesis of a Tertiary bimodal dolerite–peralkaline/subalkaline trachyte/rhyolite dyke association from Lundy, Bristol Channel, UK. *Geological Journal*, **27**, 101–117, https://doi.org/10.1002/gj.3350270202

Thorpe, R.S., Tindle, A.G. and Gledhill, A. 1990. The petrology and origin of the Tertiary Lundy granite (Bristol Channel, UK). *Journal of Petrology*, **31**, 1379–1406, https://doi.org/10.1093/petrology/31.6.1379

Troll, V.R., Nicoll, G.R., Donaldson, C.H. and Emeleus, H.C. 2008. Dating the onset of volcanism at the Rum Igneous Centre, NW Scotland. *Journal of the Geological Society, London*, **165**, 651–659, https://doi.org/10.1144/0016-76492006-190

Upton, B.G.J. 1988. History of Tertiary igneous activity in the N Atlantic borderlands. *Geological Society, London, Special Publications*, **39**, 429–453, https://doi.org/10.1144/GSL.SP.1988.039.01.38

Walsh, J.N., Beckinsale, R.D., Skelhorn, R.R. and Thorpe, R.S. 1979. Geochemistry and petrogenesis of Tertiary granitic rocks from the Island of Mull, northwest Scotland. *Contributions to Mineralogy and Petrology*, **71**, 99–116, https://doi.org/10.1007/BF00375426

Westerhold, T., Röhl, U., McCarren, H.K. and Zachos, J.C. 2009. Latest on the absolute age of the Paleocene–Eocene Thermal Maximum (PETM): new insights from exact stratigraphic position of key ash layers +19 and −17. *Earth and Planetary Science Letters*, **287**, 412–419, https://doi.org/10.1016/j.epsl.2009.08.027

Westerhold, T., Röhl, U., Frederichs, T., Agnini, C., Raffi, I., Zachos, J.C. and Wilkens, R.H. 2017. Astronomical calibration of the Ypresian timescale: implications for seafloor spreading rates and the chaotic behavior of the solar system? *Climate of the Past*, **13**, 1129–1152, https://doi.org/10.5194/cp-13-1129-2017

White, L.T. and Ireland, T.R. 2012. High-uranium matrix effect in zircon and its implications for SHRIMP U–Pb age determinations. *Chemical Geology*, **306–307**, 78–91, https://doi.org/10.1016/j.chemgeo.2012.02.025

Wiedenbeck, M., Hanchar, J.M. *et al.* 2004. Further characterisation of the 91500 Zircon crystal. *Geostandards and Geoanalytical Research*, **28**, 9–39, https://doi.org/10.1111/j.1751-908X.2004.tb01041.x

Wilkinson, C.M., Ganerød, M., Hendriks, B.W. and Eide, E.A. 2017. Compilation and appraisal of geochronological data from the North Atlantic Igneous Province (NAIP). *Geological Society, London, Special Publications*, **447**, 69–103, https://doi.org/10.1144/SP447.10

Zacke, A., Voigt, S., Joachimski, M.M., Gale, A.S., Ward, D.J. and Tütken, T. 2009. Surface-water freshening and high-latitude river discharge in the Eocene North Sea. *Journal of the Geological Society, London*, **166**, 969–980, https://doi.org/10.1144/0016-76492008-068

Zeebe, R.E. and Lourens, L.J. 2019. Solar system chaos and the Paleocene–Eocene boundary age constrained by geology and astronomy. *Science*, **365**, 926–929, https://doi.org/10.1126/science.aax0612